

Studies in Singular Optics and Coherence Theory

Studies in Singular Optics and Coherence Theory

Proefschrift

ter verkrijging van de graad van doctor
aan de Technische Universiteit Delft,
op gezag van de Rector Magnificus prof.dr.ir. J.T. Fokkema,
voorzitter van het College voor Promoties,
in het openbaar te verdedigen op
vrijdag 29 mei 2009 om 10:00 uur

door

Robert William SCHOONOVER
Master of Science in Electrical and Computer Engineering

geboren te Macomb, Illinois, USA

Dit proefschrift is goedgekeurd door de promotor:
Prof. Dr. T.D. Visser

Samenstelling promotiecommissie:
Rector Magnificus, voorzitter
Prof. dr. T.D. Visser, Technische Universiteit Delft, promotor
Prof. dr. P.S. Carney, University of Illinois at Urbana-Champaign, USA
Prof. dr. D. Lenstra, Technische Universiteit Delft
Prof. dr. L. Kuipers, Universiteit Twente
Prof. dr. ir. H. Blok, Technische Universiteit Delft
Prof. dr. ir. P.M. van den Berg, Technische Universiteit Delft

This research was sponsored by a Fulbright Scholarship.

ISBN: 978-90-9024275-0

Copyright © 2009 R.W. Schoonover

All Rights reserved. No part of this publication may be reproduced, stored in a retrieval system or transmitted in any form or by any means: electronic, mechanical, photocopying, recording or otherwise, without prior written permission of the author.

A free electronic version of this thesis can be downloaded from:

<http://www.library.tudelft.nl/dissertations>

Contents

Contents	5
1 Introduction	7
1.1 Historical introduction	7
1.2 Outline of this thesis	9
1.3 Maxwell's equations and the wave equations	10
1.4 Green functions	12
1.5 Coherence theory	13
1.6 Singular optics	14
2 The Power Radiated by Two Correlated Sources	17
2.1 Introduction	18
2.2 Primary sources	18
2.3 Secondary sources	22
3 Polarization Singularities of Focused, Radially Polarized Fields	25
3.1 Introduction	26
3.2 Focused, radially polarized fields	27
3.3 The electric energy density	28
3.4 Phase singularities of the field components	30
3.5 The state of polarization in the focal plane	30
3.6 The state of polarization in the focal region	34
3.7 Polarization singularities	38
3.7.1 Linear polarization	39
3.7.2 Circular polarization	39
3.7.3 Relationship between L -lines and C -points	42
3.7.4 Vector singularities	45
3.8 Discussion	47
4 A Cascade of Singularities in Young's Interference Experiment	49
4.1 Introduction	50

4.2	Correlation singularities and dark lines	51
4.3	Dark lines and polarization singularities	55
4.4	Conclusions	60
5	Polarization Singularities in an N-Pinhole Interferometer	61
5.1	Introduction	62
5.2	The two-pinhole interferometer	63
5.3	The three-pinhole interferometer	67
5.4	An N -pinhole interferometer	73
5.5	Conclusion	76
	Bibliography	79
	A Mathematical Derivations	87
A.1	The sign rule	87
A.2	Polarization states	88
	Summary	91
	List of Publications	93
	Biography	95
	Acknowledgments	97

Chapter 1

Introduction

1.1 Historical introduction

Physical optics is the wave-theory based study of classical optical fields. Active areas of research in physical optics include the state of polarization, the coherence properties, and the effects of propagation for an optical field [BORN AND WOLF, 1999; MANDEL AND WOLF, 1995; WOLF, 2007; BROSSEAU, 1998]. Physical optics, in contrast to geometrical optics, is based on a wave theory, rather than a ballistic theory, for the optical fields. It can be shown that geometrical optics is, in fact, a limiting case for certain types of wave fields. See [BORN AND WOLF, 1999, Chapter 3] or [BALANIS, 1989, Chapter 13] for two separate treatments.

A proper physics-based model for each of these effects is found in Maxwell's equations [MAXWELL, 1892] and the constitutive relations that relate field strengths to flux densities in various media [CHEW, 1995]. When Maxwell's equations are related in their differential form, they can be reduced to a set of wave equations for either the magnetic or electric field.

It is often the case that the fields of interest in optical research are time-harmonic fields, *i.e.* the fields oscillate at one temporal frequency, ω . By applying this assumption to the wave equations for the electric and magnetic fields, a set of Helmholtz equations is obtained. This reduction in dimensionality simplifies the problem of calculating the optical fields in space based on a set of boundary or initial conditions. The formalism of Green functions may be applied to the Helmholtz or wave equations to solve for the electric or magnetic field in all space [TAI, 1994].

Since Huyghens' experiments with calcite crystals more than 300 years ago [HUYGHENS, 1690], it has been known that light can be polarized, and the state of polarization of light has become an important area of research. Often, the state of polarization is characterized by four numbers - the Stokes parameters - that

define uniquely the polarization state of a wavefield [STOKES, 1852]. The Stokes parameters, however, are only useful in cases when the electric field is confined to a two-dimensional plane. This criterion is satisfied by plane waves and fields that are well-modeled by the paraxial approximation, *i.e.* beams. A more involved treatment is necessary when the electric field is not bound to a two-dimensional plane [HANNAY, 1998].

Statistical optics, or coherence theory [WOLF, 2007] is the branch of physical optics concerned with the properties of nondeterministic light. By applying the assumptions of stationarity and ergodicity, time-averaged measurements made by an optical detector can be related to the ensemble average over all possible realizations of the random wavefield. For nondeterministic fields, correlation functions play an important role. The two-time, two-point correlation function of a field, the mutual coherence function, is used to model broadband stochastic fields. Quasi-monochromatic fields are well-modeled by the cross-spectral density, a two-point, one-frequency function of the field. Through the Wiener-Khintchine-Einstein theorem, these two functions can be related [WIENER, 1930; KHINTCHINE, 1934; EINSTEIN, 1914].

Much like the fields themselves, the correlation functions for optical fields obey a set of propagation laws [WOLF, 1955; MANDEL AND WOLF, 1995]. The propagated versions of the correlation functions allow one to predict the results of experiments using nondeterministic light [WOLF, 2007]. This predictive capability has a wide variety of applications, including stellar interferometry [MICHELSON AND PEASE, 1921; HANBURY BROWN AND TWISS, 1954], spectroscopy [WOLF, 1986; WOLF AND JAMES, 1996], imaging [FISCHER AND CAIRNS, 1995], and focusing [WANG *et al.*, 1997; FISCHER AND VISSER, 2004].

It has recently become clear that polarization, the correlation between two electric field components at a single point, and coherence, the correlation of two electric field components of the field at two points, are intimately connected [WOLF, 2003]. It is for this reason that these two topics, coherence and polarization, are both studied in this thesis.

Singular optics [NYE AND BERRY, 1974; NYE, 1999] is a branch of wave analysis concerned with the presence of singular structures in a wavefield (field nulls, zeroes of the two-point correlation function, non-elliptical polarization) and the topology of the wavefield around those structures. For complex scalar fields, or when considering only a component of a vector field, the singular structure is a *phase* singularity [NYE AND BERRY, 1974]. Occurring at a zero of the field (or field component), a phase singularity is a point at which the phase is undefined. The region near a phase singularity is typified by a swirling (either clockwise or counter-clockwise) of the phase. Much like a phase singularity, a *coherence vortex* is a singular structure associated with a zero of the cross-spectral density [GBUR

et al., 2001]. As the cross-spectral density is of a higher dimension than the field, its behavior near a coherence vortex is only well-understood for a small subset of possible fields [GBUR AND SWARTZLANDER, 2008; VAN DIJK AND VISSER, 2009; VAN DIJK *et al.*, 2009]. For complex vector fields, a *polarization* singularity is a point, line, or surface in space at which the polarization ellipse is degenerate, *i.e.* the polarization is linear or circular [BERRY AND DENNIS, 2001]. Phase singularities of the components of a vector field represent a subset of the possible linear polarization states for a vector field. The polarization ellipses in the region near a point of circular polarization generically behave in one of three well-known ways [NYE, 1999]. The tools of singular optics can thus be applied to the analysis of a wide variety of wavefields.

1.2 Outline of this thesis

By understanding Maxwell's equations and, from them, how optical fields propagate, a number of interesting problems in optics may be studied. A field which is, in some sense, stochastic, may be treated within the confines of coherence theory, where the random field is characterized by its cross-spectral density. The cross-spectral density of the random field may be shown to obey a double Helmholtz equation, which allows one to calculate the cross-spectral density in all space based on certain boundary conditions [WOLF, 1955]. Thomas Young's famous experiment [YOUNG, 1804; YOUNG, 1807] may be better analyzed within the framework of propagating optical fields, either deterministic or stochastic [ZERNIKE, 1938]. The optical field in the focal region of a lens can likewise be found through propagation techniques based on Maxwell's equations [RICHARDS AND WOLF, 1959].

In the remainder of this Chapter, the wave equations for electric and magnetic fields are derived; the Green function for a scalar optical field is derived; the basic tenants of coherence theory are introduced; and some basic concepts in singular optics are discussed.

The total power radiated by two partially coherent sources is investigated in Chapter 2. It is found that the total power is related to the degree of coherence between the two sources and the separation between them.

In Chapter 3, the singular structures of a focused, radially-polarized field are identified. By varying the opening angle of the lens (the numerical aperture), the creation and annihilation of various singular structures are observed, including points of circular polarization, lines of linear polarization, and an unstable point in the focal region at which there is no electric field at all.

In Chapter 4, the relationship between singular structures in various optical regimes - deterministic scalar fields, deterministic vector fields, and stochastic scalar fields - are identified using a Young's interferometer. It is shown that the

mathematical structure of each wave theory results in the coincidence, on an observation screen, of singular structures for a field of each of the types listed above.

In Chapter 5, the state of polarization of a field propagating away from an N -pinhole interferometer is examined. It is shown that the presence of singular structures is generic, *i.e.* requires no symmetry of the configuration, and that any polarization state can be created when $N > 2$.

1.3 Maxwell's equations and the wave equations

The fundamental equations of electromagnetism are Maxwell's equations. In differential form, they are

$$\nabla \times \tilde{\mathbf{E}}(\mathbf{r}, t) = -\frac{\partial}{\partial t} \tilde{\mathbf{B}}(\mathbf{r}, t), \quad (1.1)$$

$$\nabla \times \tilde{\mathbf{H}}(\mathbf{r}, t) = \tilde{\mathbf{J}}(\mathbf{r}, t) + \frac{\partial}{\partial t} \tilde{\mathbf{D}}(\mathbf{r}, t), \quad (1.2)$$

$$\nabla \cdot \tilde{\mathbf{B}}(\mathbf{r}, t) = 0, \quad (1.3)$$

$$\nabla \cdot \tilde{\mathbf{D}}(\mathbf{r}, t) = \tilde{\rho}(\mathbf{r}, t), \quad (1.4)$$

where, $\tilde{\mathbf{E}}$ is the electric field, $\tilde{\mathbf{H}}$ is the magnetic field, $\tilde{\mathbf{B}}$ is the magnetic flux, $\tilde{\mathbf{D}}$ is the electric flux, $\tilde{\mathbf{J}}$ is the current density, and $\tilde{\rho}$ is the charge density. The charge and current densities are sources, and the other four quantities fully describe the electromagnetic field. It is impossible to further simplify these equations without *constitutive relations*, *i.e.* equations that relate the flux densities to the fields. The constitutive relations are functions of the material in which the electromagnetic field is propagating, and can be calculated directly [LORENTZ, 1880; LORENZ, 1881].

In the most general case, the flux densities are functionals of the fields. However, it is often true that there are linear, local, instantaneous, and isotropic relations between the flux and the field, resulting in

$$\tilde{\mathbf{D}}(\mathbf{r}, t) = \epsilon \tilde{\mathbf{E}}(\mathbf{r}, t), \quad (1.5)$$

$$\tilde{\mathbf{B}}(\mathbf{r}, t) = \mu \tilde{\mathbf{H}}(\mathbf{r}, t), \quad (1.6)$$

where ϵ is the electric permittivity and μ is the magnetic permeability.

With these constitutive relations in place, the electric and magnetic fields can be decoupled. Taking the curl of Eq. (1.1) and interchanging the order of derivatives results in

$$\nabla \times \nabla \times \tilde{\mathbf{E}}(\mathbf{r}, t) = -\frac{\partial}{\partial t} \nabla \times \tilde{\mathbf{B}}(\mathbf{r}, t). \quad (1.7)$$

Using Eq. (1.6) and substituting Eq. (1.2) for $\nabla \times \tilde{\mathbf{B}}(\mathbf{r}, t)$ results in

$$\nabla \times \nabla \times \tilde{\mathbf{E}}(\mathbf{r}, t) = -\mu \frac{\partial^2}{\partial t^2} \tilde{\mathbf{D}}(\mathbf{r}, t) - \mu \frac{\partial}{\partial t} \tilde{\mathbf{J}}(\mathbf{r}, t). \quad (1.8)$$

By substituting from Eq. (1.5), one arrives at the uncoupled equation for the electric field:

$$\nabla \times \nabla \times \tilde{\mathbf{E}}(\mathbf{r}, t) + \epsilon \mu \frac{\partial^2}{\partial t^2} \tilde{\mathbf{E}}(\mathbf{r}, t) = -\mu \frac{\partial}{\partial t} \tilde{\mathbf{J}}(\mathbf{r}, t). \quad (1.9)$$

Finally, using the vector relationship $\nabla \times \nabla \times \mathbf{A} = \nabla(\nabla \cdot \mathbf{A}) - \nabla^2 \mathbf{A}$, the wave equation for the electric field is found, *viz*,

$$\nabla^2 \tilde{\mathbf{E}}(\mathbf{r}, t) - \mu \epsilon \frac{\partial^2}{\partial t^2} \tilde{\mathbf{E}}(\mathbf{r}, t) = \mu \frac{\partial}{\partial t} \tilde{\mathbf{J}}(\mathbf{r}, t) + \frac{1}{\epsilon} \nabla \tilde{\rho}(\mathbf{r}, t). \quad (1.10)$$

In an analogous manner, the wave equation for the magnetic field can be derived. This results in

$$\nabla^2 \tilde{\mathbf{H}}(\mathbf{r}, t) - \mu \epsilon \frac{\partial^2}{\partial t^2} \tilde{\mathbf{H}}(\mathbf{r}, t) = -\nabla \times \tilde{\mathbf{J}}(\mathbf{r}, t). \quad (1.11)$$

One can immediately identify the speed with which the electric and magnetic fields propagate as $c = 1/\sqrt{\mu\epsilon}$. Light is thus an electromagnetic disturbance, and the state of polarization is defined entirely by the vector $\mathbf{E}(\mathbf{r}, \omega)$. Note that this result does not take into account the possibility of an inhomogeneous medium, *i.e.* there are no scatterers present, just sources.

Often, one is interested in time-harmonic fields, that is, fields that oscillate at a single frequency. The fields are generated by time-harmonic sources. The electric field and the source densities can thus be written as

$$\begin{aligned} \tilde{\mathbf{E}}(\mathbf{r}, t) &= \mathbf{E}(\mathbf{r}, \omega) e^{-i\omega t}, \\ \tilde{\mathbf{J}}(\mathbf{r}, t) &= \mathbf{J}(\mathbf{r}, \omega) e^{-i\omega t}, \\ \tilde{\rho}(\mathbf{r}, t) &= \rho(\mathbf{r}, \omega) e^{-i\omega t}. \end{aligned} \quad (1.12)$$

Substituting Eq. (1.12) into Eq. (1.10), one obtains the Helmholtz equation for the electric field,

$$\nabla^2 \mathbf{E}(\mathbf{r}, \omega) + k_0^2 \mathbf{E}(\mathbf{r}, \omega) = -i\omega \mu \mathbf{J}(\mathbf{r}, \omega) + \frac{1}{\epsilon} \nabla \rho(\mathbf{r}, \omega), \quad (1.13)$$

where $k_0 = \omega/c$, where c is the speed of light. When the field is linearly polarized, or when the field is unpolarized, a scalar approximation may be valid for describing the electric (or magnetic) field. The Helmholtz equation for scalar fields is

$$\nabla^2 U(\mathbf{r}, \omega) + k_0^2 U(\mathbf{r}, \omega) = -4\pi \kappa(\mathbf{r}, \omega), \quad (1.14)$$

where κ is the source density. A scalar approximation for optical fields is often used in coherence theory and in many scattering and imaging problems.

1.4 Green functions

A differential equation such as Eq. (1.14) defines a local relationship between the field at given point and the source terms. The solution to that differential equation, however, defines the field at all points in the region. The method of Green functions is used to calculate the field based on the sources and certain boundary conditions.

Consider the two equations

$$\nabla^2 G(\mathbf{r}, \mathbf{r}'; \omega) + k_0^2 G(\mathbf{r}, \mathbf{r}'; \omega) = -4\pi\delta(\mathbf{r} - \mathbf{r}'), \quad (1.15)$$

$$\nabla^2 U(\mathbf{r}, \omega) + k_0^2 U(\mathbf{r}, \omega) = -4\pi\kappa(\mathbf{r}, \omega), \quad (1.16)$$

where \mathbf{r}' is an arbitrary point in the region of interest. Multiplying both sides of Eq. (1.15) by U and both sides of Eq. (1.16) by G and taking the difference, one gets,

$$\begin{aligned} & U(\mathbf{r}, \omega)\nabla^2 G(\mathbf{r}, \mathbf{r}'; \omega) - G(\mathbf{r}, \mathbf{r}'; \omega)\nabla^2 U(\mathbf{r}, \omega) \\ &= -4\pi\delta(\mathbf{r} - \mathbf{r}')U(\mathbf{r}, \omega) + 4\pi\kappa(\mathbf{r}, \omega)G(\mathbf{r}, \mathbf{r}'; \omega). \end{aligned} \quad (1.17)$$

Integrating over the unprimed variables, and applying Green's theorem yields

$$\begin{aligned} & \oint_{\partial\mathcal{V}} d\mathbf{S} \cdot [U(\mathbf{r}, \omega)\nabla G(\mathbf{r}, \mathbf{r}'; \omega) - G(\mathbf{r}, \mathbf{r}'; \omega)\nabla U(\mathbf{r}, \omega)] \\ &= -4\pi U(\mathbf{r}', \omega) + 4\pi \int_{\mathcal{V}} d^3r G(\mathbf{r}, \mathbf{r}'; \omega)\kappa(\mathbf{r}, \omega), \end{aligned} \quad (1.18)$$

where $d\mathbf{S}$ is the outward-pointing differential surface element along the boundary of the region of interest, \mathcal{V} . One sees that both the source and the field at the boundary contribute to the field in the region. The boundary conditions are system-dependent. For example, a perfect conductor has the boundary condition $U(\mathbf{r}, \omega) = 0 \quad \forall \mathbf{r} \in \partial\mathcal{V}$.

The Green function of Eq. (1.15) can often be chosen so that one of the terms inside the surface integral in Eq. (1.18) is identically zero. Thus, the field can be found anywhere in the region \mathcal{V} through knowledge of the field or its derivative on the boundary of the region and the source density. In free space, the Green function obeys the boundary condition known as the Sommerfeld radiation condition and is of the form

$$G(\mathbf{r}, \mathbf{r}'; \omega) = \frac{e^{ik|\mathbf{r}-\mathbf{r}'|}}{|\mathbf{r} - \mathbf{r}'|}. \quad (1.19)$$

A similar method can be used to calculate the electric field [TAI, 1994] or the correlation functions of a stochastic field [WOLF, 1955] within a specified region.

1.5 Coherence theory

A random process, $x(t)$, is considered to be wide-sense stationary if the statistics up to second order are time-shift invariant, *i.e.* $\langle x^*(t_1)x(t_2) \rangle = \langle x^*(t_1+\tau)x(t_2+\tau) \rangle$ for any time shift, τ , where $\langle \cdot \rangle$ denotes an ensemble average. In the case of ergodic fields, the ensemble average can be replaced with a time average [WOLF, 2007]. One notes that the autocorrelation, $\Gamma(t_2 - t_1) = \langle x^*(t_1)x(t_2) \rangle$, is a function only of the time difference. The Fourier transform of the two-time autocorrelation is a well-defined quantity:

$$\iint dt_1 dt_2 \Gamma(t_2 - t_1) e^{i(\omega t_2 - \omega' t_1)} = S(\omega) \delta(\omega - \omega'), \quad (1.20)$$

where $S(\omega)$ is the spectral density. This relationship, known as the Wiener-Khintchine-Einstein theorem [WIENER, 1930; KHINTCHINE, 1934; EINSTEIN, 1914], shows that a wide-sense stationary field is uncorrelated across any two distinct frequencies, and that a measurement of the spectral densities allows one to find the correlation function of the random field.

A collection of random processes, $\{x_n(t)\}$, are considered to be jointly stationary (at least in the wide sense), if for any two wide-sense stationary random processes, the cross-correlation between those processes is also only a function of the time difference: $\Gamma_{ij}(t_2 - t_1) = \langle x_n^*(t_1)x_j(t_2) \rangle$ for all x_i and x_j . A stationary optical source is a collection of jointly-stationary, wide-sense stationary stochastic emitters. In cases of practical importance, the cross-correlation for the field is an important quantity, and can be written as $\Gamma_{ij} = \langle x_i^*(t_1)x_j(t_2) \rangle$. As a generalization of the Wiener-Khintchine-Einstein theorem, the cross-spectral density for the collection of sources is given by the formula

$$W_{ij}(\omega)\delta(\omega - \omega') = \iint dt_1 dt_2 \Gamma_{ij}(t_2 - t_1) e^{i(\omega t_2 - \omega' t_1)}. \quad (1.21)$$

One can also consider the cross-spectral density to be the ensemble average of a collection of stochastic frequency-domain fields, that is $W_{ij}(\omega)\delta(\omega - \omega') = \langle X_i^*(\omega')X_j(\omega) \rangle$ [WOLF, 1981; WOLF, 1982]. It is important to note that the collection of temporal fields $\{x_n(t)\}$ and the collection of frequency-domain fields $\{X_m(\omega)\}$ are *not* related by a Fourier transform. There is also no specified relationship between any elements of the ensemble of temporal fields and the ensemble of frequency-domain fields.

An important quantity in coherence theory is the spectral degree of coherence between two sources. It is a complex number with magnitude between zero and one, and is defined as

$$\mu_{ij}(\omega) = \frac{W_{ij}(\omega)}{\sqrt{W_{ii}(\omega)W_{jj}(\omega)}}. \quad (1.22)$$

The spectral degree of coherence conveys the degree of statistical similarity between the fields emanating from sources i and j . When $|\mu_{ij}| = 1$, the two sources are called 'fully coherent.' When $|\mu_{ij}| = 0$, the two sources are 'incoherent.' All other values of the degree of coherence imply that the two sources are 'partially coherent.'

1.6 Singular optics

Singular optics [NYE, 1999; SOSKIN AND VASNETSOV, 2001] is the branch of physical optics concerned with points in a wavefield in which some quantity, usually the phase of a complex field, is undefined. Consider the function $f(\mathbf{r}) = A(\mathbf{r}) \exp(i\phi(\mathbf{r}))$, where A and ϕ are real-valued functions. Suppose that, at the point \mathbf{r}' , $A(\mathbf{r}') = 0$. The function ϕ is thus undefined at \mathbf{r}' , and \mathbf{r}' is a singular point for f , also known as a phase singularity. The charge of a phase singularity, s , is defined by the relation

$$s = \frac{1}{2\pi} \oint_C \nabla\phi(\mathbf{r}) \cdot d\mathbf{r}, \quad (1.23)$$

where the path C encloses the phase singularity and is taken in the counter-clockwise direction [NYE, 1999].

In the case that the field of interest is a two-dimensional real-valued vector field, $\mathbf{B}(\mathbf{r})$, the phase is defined as $\phi = \tan^{-1}(B_y/B_x)$ [SCHOUTEN *et al.*, 2003c; SCHOUTEN *et al.*, 2004a]. For complex two-dimensional fields, there are a collection of singular structures - points in which the field is linearly polarized, known as L -points; points in which the field is circularly polarized, known as C -points; and points at which the complex field is identically zero, or V -points [BERRY AND DENNIS, 2001].

The location of the singular structures in a wavefield are often a function of some system parameter. For focused fields, the parameter may be the semi-aperture angle of the lens [DIEHL *et al.*, 2006; SCHOONOVER AND VISSER, 2006]. For an N -pinhole experiment, the pinhole separation distance, the phase relationship between the fields in each pinhole, and the orientation angle of the field in each pinhole (for vector fields) may be used [GBUR *et al.*, 2001; VISSER AND SCHOONOVER, 2008; GAN AND GBUR, 2007; GBUR *et al.*, 2004a; SCHOUTEN *et al.*, 2004a; RUBEN AND PAGANIN, 2007]. For any of these cases, the system parameter can be smoothly changed, and the location of the singular structures will move. In the event that this movement causes two singularities to collide, one of two things may happen: if the singularities are of the same type and of opposite charge, they will annihilate, leaving no singularities; if the two singularities are of differing types (a left-handed and right-handed C -point), the resulting collision

will result in a V -point. As the system parameter is changed, it is also possible that pairs of phase singularities will appear and move apart. This process is known as the creation of phase singularities.

The creation and annihilation of phase singularities are two complementary processes - reversing the way in which the system parameter is smoothly changed will turn the creation process into an annihilation and *vice versa*. The complementary process to the creation of a V -point is the unfolding of that V -point into a number of singular structures. This process has been investigated for focused fields [SCHOONOVER AND VISSER, 2006] and the field emanating from a two-pinhole experiment [VISSER AND SCHOONOVER, 2008].

The tools and results of singular optics are useful in many applications. Because of their use in, for example, optical trapping, the properties of focused, radially polarized beams have been studied extensively in the past few years (see, e.g., [VISSER AND FOLEY, 2005] and the references therein). By locating points where either the radial or longitudinal component of the focused field is zero, improvements may be made in the trapping scheme. The control of polarization states is important in many imaging problems [DAVIS AND CARNEY, 2008], and thus the ability to define and control the state of polarization for a wavefield has many uses. Analysis of the singularities of the Poynting vector can be used to enhance the transmission of light through small apertures [SCHOUTEN *et al.*, 2003b; SCHOUTEN *et al.*, 2003c; SCHOUTEN *et al.*, 2004b].

Chapter 2

The Power Radiated by Two Correlated Sources

This Chapter is based on the following publication:

- **R.W. Schoonover**, T.D. Visser, “The power radiated by two correlated sources,” *Opt. Commun.* **271**, Issue 2, 323–326 (2007).

Abstract

We analyze the total power that is radiated by two correlated point sources. The influence of the degree of coherence between the two sources and of the distance between them can clearly be distinguished. Significant modulations of the total radiated power are predicted. Both primary and secondary sources are investigated.

2.1 Introduction

When the light from two point sources interferes, as, for example, in Thomas Young's celebrated experiment [BORN AND WOLF, 1999; SCHOUTEN *et al.*, 2004a], the visibility of the interference fringes that are formed is a direct measure of the correlation between the source fields [ZERNIKE, 1938]. The *spectral interference law* expresses how the spectral density (or 'spectral intensity') at an observation point in the region of superposition depends on the *spectral degree of coherence* [MANDEL AND WOLF, 1995, Sec. 4.3.2].

In this Chapter we study the total power that is radiated by two correlated point sources. As we will demonstrate, the power is modulated significantly by both the distance between the two sources, and by their spectral degree of coherence. Especially when the distance between the two sources is of the order of a wavelength, a situation that is commonly found in acoustics, strong modulations are predicted. Further testimony to the relevance of our study is that after completion of the manuscript we discovered its resemblance to a more restricted research problem suggested in [MANDEL AND WOLF, 1995] of which the solution has never been published. Our analysis treats both primary and secondary sources. We illustrate our findings with numerical results.

2.2 Primary sources

Consider two identical, small primary sources located at points Q_1 and Q_2 , that are separated by a vector \mathbf{d} . Let $S_Q(\omega)$ be the spectrum of each source, ω being an angular frequency. The field at an observation point P is then given by the formula

$$U(P, \omega) = U(Q_1, \omega) \frac{e^{ikR_1}}{R_1} + U(Q_2, \omega) \frac{e^{ikR_2}}{R_2}, \quad (2.1)$$

where R_i is the distance between Q_i and P ($i = 1, 2$), and $k = \omega/c$ with c the speed of light in vacuum. If the spectral degree of coherence between the two source fields is denoted by $\mu_Q(\omega)$, then the spectral density at P is given by

$$S(P, \omega) = \langle U^*(P, \omega) U(P, \omega) \rangle, \quad (2.2)$$

$$= S_Q(\omega) \left\{ \frac{1}{R_1^2} + \frac{1}{R_2^2} + \left[\mu_Q(\omega) \frac{e^{ik(R_2-R_1)}}{R_1 R_2} + \text{c.c.} \right] \right\}. \quad (2.3)$$

Here c.c. is the complex conjugate, and the angle brackets denote an average taken over an ensemble of source field realizations (in the sense of coherence theory in the space-frequency domain [MANDEL AND WOLF, 1995, Ch. 4]) that are assumed

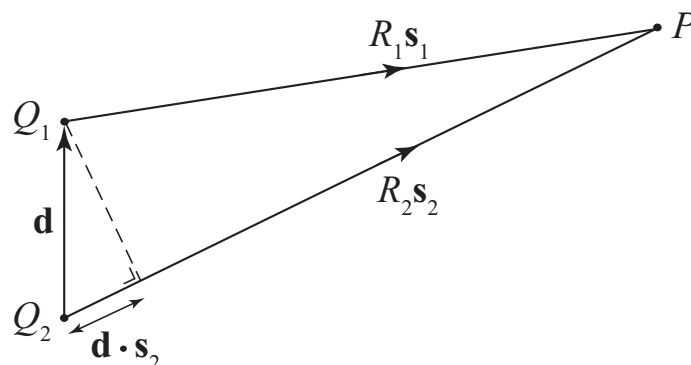


Figure 2.1: Illustrating the notation relating to the far-zone approximation (2.6).

to be stationary, at least in the wide sense. The spectral degree of coherence of the two source fields satisfies the relation

$$\mu_Q(\omega) = \frac{W_Q(Q_1, Q_2; \omega)}{S_Q(\omega)}, \quad (2.4)$$

with

$$W_Q(Q_1, Q_2; \omega) = \langle U^*(Q_1, \omega)U(Q_2, \omega) \rangle \quad (2.5)$$

being the cross-spectral density of the two source fields. When the point P is in the far zone, we have to a good approximation (see Fig. 2.1),

$$\frac{e^{ik(R_2-R_1)}}{R_1R_2} \approx \frac{e^{ik\mathbf{d}\cdot\mathbf{s}_2}}{R_2^2}, \quad (2.6)$$

with \mathbf{s}_2 a unit vector. On substituting from Eq. (2.6) into Eq. (2.3) we obtain for the far-zone spectrum the formula

$$S^{(\infty)}(P, \omega) = \frac{S_Q(\omega)}{R_2^2} \{2 + [\mu_Q(\omega)e^{ik\mathbf{d}\cdot\mathbf{s}_2} + \text{c.c.}]\}. \quad (2.7)$$

Suppressing the subscript 2 and writing $S^{(\infty)}(R\mathbf{s}, \omega)$ rather than $S^{(\infty)}(P, \omega)$, Eq. (2.7) becomes

$$S^{(\infty)}(R\mathbf{s}, \omega) = \frac{S_Q(\omega)}{R^2} \{2 + [\mu_Q(\omega)e^{ik\mathbf{d}\cdot\mathbf{s}} + \text{c.c.}]\}. \quad (2.8)$$

On integrating this result over all possible angles we find for the total power that is radiated by two correlated primary point sources the expression

$$P(\omega) = R^2 \int_{(4\pi)} S^{(\infty)}(R\mathbf{s}, \omega) d\Omega, \quad (2.9)$$

$$= 2S_Q(\omega) \left\{ 4\pi + \left[\frac{1}{2} \mu_Q(\omega) \int_{(4\pi)} e^{i\mathbf{k}\mathbf{d}\cdot\mathbf{s}} d\Omega + \text{c.c.} \right] \right\}, \quad (2.10)$$

$$= 8\pi S_Q(\omega) [1 + j_0(kd) \text{Re}\{\mu_Q(\omega)\}], \quad (2.11)$$

where Re denotes the real part, $d = |\mathbf{d}|$ and j_0 is the spherical Bessel function of the first kind and of order zero. It is seen from Eq. (2.11) that *the total power that is radiated at frequency ω consists of the sum of the contributions of the two sources, and an interference term which depends on both the spectral degree of coherence of the two source fields, $\mu_Q(\omega)$, and on the separation between the two sources.*

Let us now discuss the implications of Eq. (2.11) for two limiting cases. First, when the separation between the two sources is much smaller than the wavelength, i.e. when $d \ll \lambda$, then

$$j_0(kd) \approx 1, \quad (2.12)$$

and Eq. (2.11) gives

$$P(\omega) \approx 8\pi S_Q(\omega) [1 + \text{Re}\{\mu_Q(\omega)\}]. \quad (2.13)$$

Since

$$-1 \leq \text{Re}\{\mu_Q(\omega)\} \leq 1, \quad (2.14)$$

we see that in this case

$$0 \leq P(\omega) \leq 16\pi S_Q(\omega). \quad (2.15)$$

If the two sources are completely uncorrelated, i.e. if $\mu_Q(\omega) = 0$, then, according to Eq. (2.11),

$$P(\omega)_{\text{uncorr.}} = 8\pi S_Q(\omega). \quad (2.16)$$

Hence we may rewrite the inequality (2.15) as

$$0 \leq P(\omega) \leq 2P(\omega)_{\text{uncorr.}}. \quad (2.17)$$

In the case when $P(\omega) = 0$ there is obviously complete cancellation of the far field due to destructive interference. Since $S^{(\infty)}(R\mathbf{s}, \omega) \geq 0$, this implies, according to Eq. (2.9), that $S^{(\infty)}(R\mathbf{s}, \omega) = 0$ for all directions \mathbf{s} . So the system

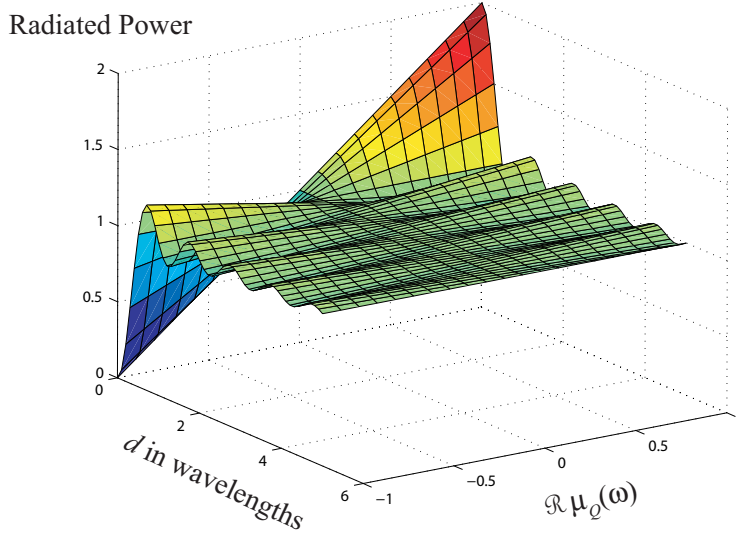


Figure 2.2: The normalized power $P(\omega)/P(\omega)_{\text{uncorr.}}$ radiated by two primary sources as a function of their separation distance d , and the real part of their spectral degree of coherence $\text{Re}\{\mu_Q(\omega)\}$.

behaves as a *non-radiating source* [GBUR, 2003]. In the other limiting case, when $P(\omega) = 2P(\omega)_{\text{uncorr.}}$, there is an increase in the radiated power due to constructive interference and, consequently the far-field spectral density in the far zone averaged over all directions is increased.

In the limit when the separation between the two sources is much larger than the wavelength, i.e. when $d \gg \lambda$, then

$$j_0(kd) \approx 0, \quad (2.18)$$

and Eq. (2.11) gives

$$P(\omega) \approx P(\omega)_{\text{uncorr.}}. \quad (2.19)$$

It is seen from Eq. (2.19) that for separation distances much greater than the wavelength, the total radiated power is independent of the spectral degree of coherence of the fields generated by the two sources.

Fig. 2.2 shows the behavior of the total power radiated by the two sources as a function of their separation distance d (in units of wavelengths) and the real part of their spectral degree of coherence $\text{Re}\{\mu_Q(\omega)\}$. Especially when the source separation is of the order of a wavelength (a situation that is commonly found, for example, in acoustics) both parameters strongly modulate the radiated power.

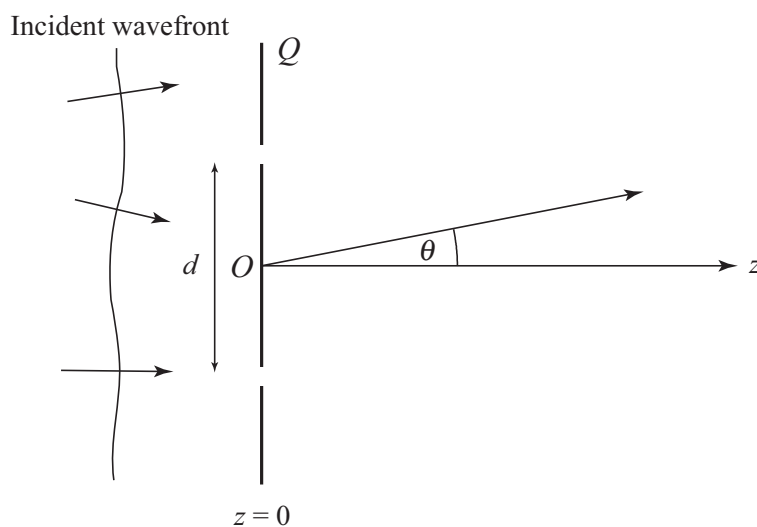


Figure 2.3: Two secondary sources.

2.3 Secondary sources

Consider an opaque screen Q , located in the plane $z = 0$, with two pinholes of radius a centered at the points specified by the vectors $\mathbf{x} = (d/2, 0, 0)$ and $-\mathbf{x}$ (see Fig. 2.3). The secondary source field in each aperture is $U_i(\omega)$, with $i = 1, 2$. Again the spectral densities are assumed to be equal, namely $S_Q(\omega)$. The field at the screen is thus given by the expression

$$U_Q(\boldsymbol{\rho}, \omega) = U_1(\omega) \text{circ}(\boldsymbol{\rho} + \mathbf{x}) + U_2(\omega) \text{circ}(\boldsymbol{\rho} - \mathbf{x}), \quad (2.20)$$

where $\boldsymbol{\rho} = (x, y, 0)$ denotes a position vector of a point in the plane $z = 0$, and

$$\text{circ}(\boldsymbol{\rho}) = \begin{cases} 1 & |\boldsymbol{\rho}| \leq a \\ 0 & |\boldsymbol{\rho}| > a. \end{cases} \quad (2.21)$$

The cross-spectral density of the field at in the plane of the screen is, therefore, given by the expression

$$W_Q(\boldsymbol{\rho}_1, \boldsymbol{\rho}_2; \omega) = \langle [U_1^*(\omega) \text{circ}(\boldsymbol{\rho}_1 + \mathbf{x}) + U_2^*(\omega) \text{circ}(\boldsymbol{\rho}_1 - \mathbf{x})] \\ \times [U_1(\omega) \text{circ}(\boldsymbol{\rho}_2 + \mathbf{x}) + U_2(\omega) \text{circ}(\boldsymbol{\rho}_2 - \mathbf{x})] \rangle, \quad (2.22)$$

The *radiant intensity* of the far-field in a direction indicated by the unit vector \mathbf{s} is related to this cross-spectral density by the equation [MANDEL AND WOLF,

1995, Eq. (5.3–8)]

$$J(\mathbf{s}, \omega) = \left(\frac{k}{2\pi}\right)^2 \cos^2 \theta \times \iint_{-\infty}^{\infty} W_Q(\boldsymbol{\rho}_1, \boldsymbol{\rho}_2; \omega) \exp[-ik\mathbf{s}_\perp \cdot (\boldsymbol{\rho}_2 - \boldsymbol{\rho}_1)] d^2\rho_1 d^2\rho_2, \quad (2.23)$$

where θ is the angle that \mathbf{s} makes with the positive z -axis, and $\mathbf{s}_\perp = (s_x, s_y)$. On substituting from Eq. (2.22) into Eq. (2.23) we find that

$$J(\mathbf{s}, \omega) = a^2 J_1^2(ka) \cos^2 \theta S_Q(\omega) \times \{2 + [\mu_Q(\omega) \exp(-iks_x d) + \text{c.c.}]\}. \quad (2.24)$$

It is seen from Eq. (2.24) that for source radii a such that $J_1(ka) = 0$ the radiant intensity vanishes identically. It is to be noted that this is not due to interference between the two sources, because in this case both sources themselves are non-radiating. The observation that for certain sizes a coherent source does not radiate at all was first made by Carter and Wolf [CARTER AND WOLF, 1981].

The total power, at frequency ω , that is radiated by the sources is given by the formula [MANDEL AND WOLF, 1995, Eq. 5.7–53]

$$P(\omega) = \int_0^{2\pi} \int_0^{\pi/2} J(\mathbf{s}, \omega) \sin \theta d\theta d\phi. \quad (2.25)$$

Now $s_x = \sin \theta \cos \phi$; on using this expression and also that

$$3 \int_0^{\pi/2} J_0(kd \sin \theta) \cos^2 \theta \sin \theta d\theta = 3 \left[\frac{\sin kd - kd \cos kd}{(kd)^3} \right], \quad (2.26)$$

$$= j_0(kd) + j_2(kd), \quad (2.27)$$

we find for the total power that is radiated at frequency ω by two correlated secondary sources the expression

$$P(\omega) = \frac{4\pi}{3} a^2 J_1^2(ka) S_Q(\omega) \{1 + [j_0(kd) + j_2(kd)] \text{Re}\{\mu_Q(\omega)\}\}, \quad (2.28)$$

Regarding Eq. (2.28) it is of interest to remark that $-1 \leq j_0(x) + j_2(x) \leq 1$.

The structure of Eq. (2.11), which pertains to primary sources, and Eq. (2.28), which pertains to secondary sources, is rather similar. One difference is that the dependence on the source separation distance is through a single spherical Bessel function of the first kind in one case, and through a sum of two such functions in the other case. The behavior of these functions is illustrated in Fig. 2.4. It is seen

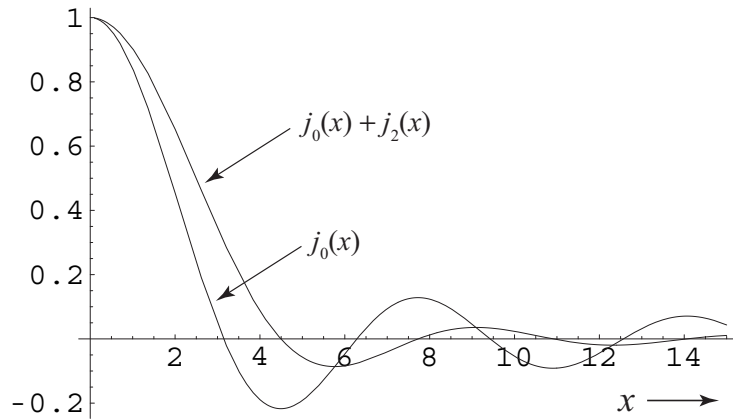


Figure 2.4: Spherical Bessel functions of the first kind.

that the interference term for two primary sources has zeros for different values of the separation distance than the interference term for two secondary sources. However, the behavior of the total power that is radiated in the limiting cases of $d \ll \lambda$ and $d \gg \lambda$ is the same for pairs of sources of both types.

In conclusion, we have derived expressions for the total power that is radiated by a pair of correlated, primary and secondary sources. The expressions consist of a direct contribution from each source and an interference term. The latter is the product of two factors: the real part of the spectral degree of coherence, and an oscillating function of the distance between the sources. When the separation distance is small compared to the wavelength – a situation that is commonly met in acoustics – the modulating influence of the degree of coherence and of the separation distance can be quite significant.

Chapter 3

Polarization Singularities of Focused, Radially Polarized Fields

This Chapter is based on the following publications:

- D.W. Diehl, **R.W. Schoonover**, and T.D. Visser, “The structure of focused, radially polarized fields,” *Opt. Express* **14**, 3030–3038 (2006).
- **R.W. Schoonover** and T.D. Visser, “Polarization singularities of focused, radially polarized fields,” *Opt. Express* **14**, 5733–5745 (2006).

Abstract

The state of polarization of strongly focused, radially polarized electromagnetic fields is examined. It is found that several types of polarization singularities exist. Their relationship is investigated, and it is demonstrated that on smoothly varying a system parameter, such as the aperture angle of the lens, different polarization singularities can annihilate each other. For example, the evolution of a lemon into a monstar and its subsequent annihilation with a star is studied. Also, the quite rare collision of a *C*-line and an *L*-line is observed.

3.1 Introduction

At points in complex-valued scalar fields where the amplitude is zero, the phase of the field is undetermined or singular [NYE AND BERRY, 1974]. Singular optics is concerned with the description and classification of the different kinds of singularities that can occur in wave fields [NYE, 1999; SOSKIN AND VASNETSOV, 2001]. Examples of such singularities are the zeros of intensity that are found in focused fields [KARMAN *et al.*, 1997]. In real-valued, two-dimensional vector fields, the orientation of the vector is singular wherever the vector vanishes. Such singularities of the Poynting vector field in two-dimensional geometries are studied in Refs. [SCHOUTEN *et al.*, 2003c; SCHOUTEN *et al.*, 2004b]. Complex-valued vector fields can display singularities of the vector components. An example of these are singularities of the longitudinal component of the electric field in strongly focused, linearly polarized beams [DIEHL AND VISSER, 2004]. Recently, the two-point correlation functions that describe spatially partially coherent light were shown to possess singularities as well [SCHOUTEN *et al.*, 2003a; GBUR AND VISSER, 2003; FISCHER AND VISSER, 2004; GBUR AND VISSER, 2005]. All types of singularities mentioned above can be created or annihilated when a system parameter, such as the wavelength of the field, is smoothly varied. In these creation/annihilation events topological charge and topological index are conserved.

At every point in a time-harmonic electromagnetic field, the end point of the electric field vector traces out an ellipse as time progresses [BORN AND WOLF, 1999, Sec. 1.4]. The polarization is said to be singular at points where this ellipse degenerates into a circle (at so-called *C*-points) or into a line (at so-called *L*-lines). Polarization singularities in wave fields are described in [NYE, 1999; BERRY AND DENNIS, 2001; FREUND *et al.*, 2002; SOSKIN *et al.*, 2003; MOKHUN *et al.*, 2002].

Because of their use in, for example, optical trapping, the properties of focused, radially polarized beams have been studied extensively in the past few years (see, e.g., [VISSER AND FOLEY, 2005] and the references therein). The electric field in the focal region of such a beam has two non-zero parts, namely a radial component and a longitudinal component. The creation and annihilation of phase singularities of these field components has been described in [DIEHL *et al.*, 2006]. In the present paper the rich polarization behavior of focused, radially polarized fields is analyzed. It is shown that the focal region contains different kinds of polarization singularities such as *L*-lines, stars, monstars, lemons, and *V*-points. Their interrelation is examined, and it is demonstrated how polarization singularities can be created or annihilated when, e.g., the semi-aperture angle of the focusing system is changed.

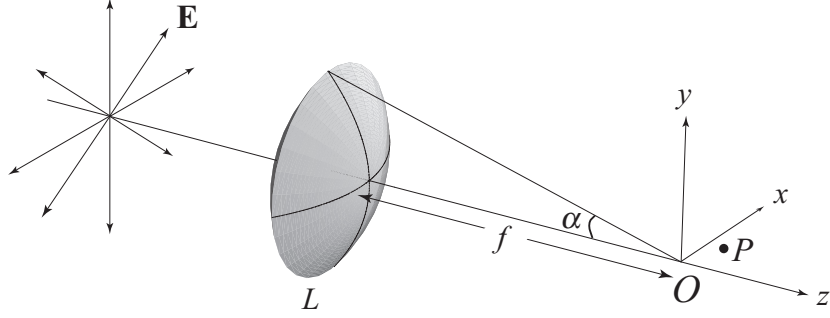


Figure 3.1: Illustration of a high numerical aperture system focusing a radially polarized beam.

3.2 Focused, radially polarized fields

Consider an aplanatic focusing system L , as depicted in Fig. 3.1. The system has a focal length f and a semi-aperture angle α . The origin O of a right-handed cartesian coordinate system is taken to be at the geometrical focus. A monochromatic, radially polarized beam is incident on the system.

The electric and magnetic fields at time t at position \mathbf{r} are given by the expressions

$$\mathbf{E}(\mathbf{r}, t) = \text{Re} [\mathbf{e}(\mathbf{r}) \exp(-i\omega t)], \quad (3.1)$$

$$\mathbf{H}(\mathbf{r}, t) = \text{Re} [\mathbf{h}(\mathbf{r}) \exp(-i\omega t)], \quad (3.2)$$

respectively, where Re denotes the real part. The longitudinal component e_z and the radial component e_ρ of the electric field at a point $P = (\rho_P, z_P)$ in the focal region are given by the equations [VISSER AND FOLEY, 2005]

$$e_z(\rho_P, z_P) = -ikf \int_0^\alpha l(\theta) \sin^2 \theta \cos^{1/2} \theta \times \exp(ikz_P \cos \theta) J_0(k\rho_P \sin \theta) d\theta, \quad (3.3)$$

$$e_\rho(\rho_P, z_P) = -kf \int_0^\alpha l(\theta) \sin \theta \cos^{3/2} \theta \times \exp(ikz_P \cos \theta) J_1(k\rho_P \sin \theta) d\theta, \quad (3.4)$$

where J_i is the Bessel function of the first kind of order i . Also, $l(\theta)$ denotes the angular amplitude function

$$l(\theta) = f \sin \theta \exp[-f^2 \sin^2 \theta / w_0^2], \quad (3.5)$$

where w_0 is the spot size of the beam in the waist plane, which is assumed to coincide with the entrance plane of the focusing system. As stated above, the electric field has no azimuthal component. On using the dimensionless optical coordinates (sometimes referred to as *Lommel variables*)

$$u = kz_P \sin^2 \alpha, \quad (3.6)$$

$$v = k\rho_P \sin \alpha, \quad (3.7)$$

to specify the position of the observation point P , Eqs. (3.3) and (3.4) can be rewritten as

$$e_z(u, v) = -ikf^2 \int_0^\alpha \sin^3 \theta \cos^{1/2} \theta \exp(-\beta^2 \sin^2 \theta) \\ \times \exp(iu \cos \theta / \sin^2 \alpha) J_0 \left(\frac{v \sin \theta}{\sin \alpha} \right) d\theta, \quad (3.8)$$

$$e_\rho(u, v) = -kf^2 \int_0^\alpha \sin^2 \theta \cos^{3/2} \theta \exp(-\beta^2 \sin^2 \theta) \\ \times \exp(iu \cos \theta / \sin^2 \alpha) J_1 \left(\frac{v \sin \theta}{\sin \alpha} \right) d\theta, \quad (3.9)$$

where the parameter $\beta = f/w_0$ denotes the ratio of the focal length of the system and the spot size of the beam in the waist plane.

3.3 The electric energy density

The time-averaged electric energy density consists of the sum of two contributions, viz.

$$w_e = \frac{\epsilon_0}{2} \mathbf{E}^2(u, v) = \frac{\epsilon_0}{4} [|e_\rho(u, v)|^2 + |e_z(u, v)|^2], \quad (3.10)$$

where ϵ_0 denotes the permittivity in vacuum. One expects the relative contribution of the longitudinal field component to increase when the semi-aperture angle α increases. It is found that this is indeed the case. In Fig. 3.2 contours of the time-averaged electric energy densities $|e_\rho(u, v)|^2$ and $|e_z(u, v)|^2$ are shown, both normalized to the same value. In this example $\alpha = \pi/6$, and it is seen that the contribution of the radial field component dominates at most points. The reverse is true, however, for larger values of α . This is illustrated in Fig. 3.3 in which contours for the same two energy density contributions are shown for the case that the semi-aperture angle $\alpha = \pi/3$. Then the contribution of the longitudinal field component is clearly dominant at most points in the focal region. These results are in agreement with earlier observations [YOUNGWORTH AND BROWN, 2000; NOVOTNY *et al.*, 2001].

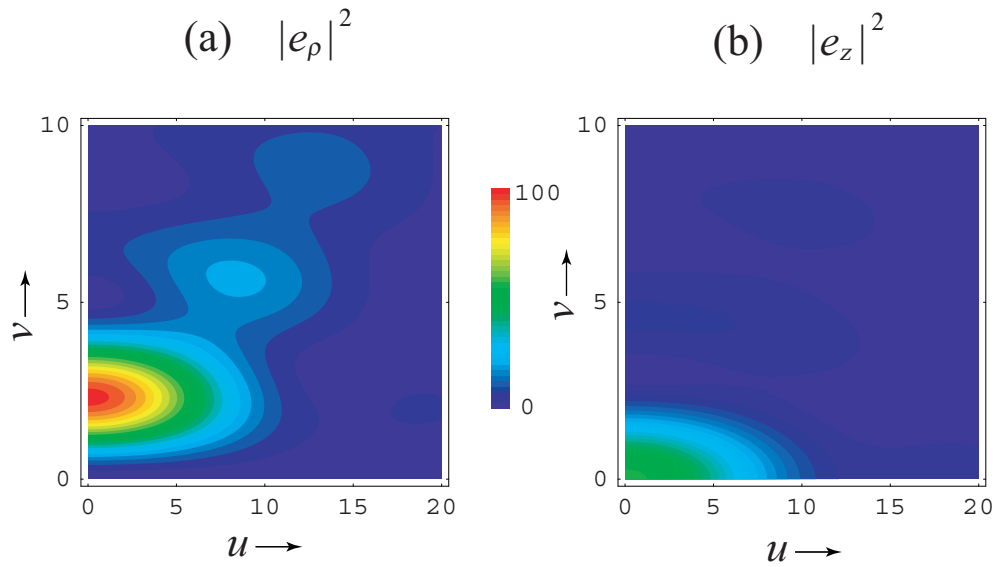


Figure 3.2: Contours of $|e_\rho(u, v)|^2$ (a) and $|e_z(u, v)|^2$ (b). In this example the semi-aperture angle $\alpha = \pi/6$, and the beam parameter $\beta = 0.6$.

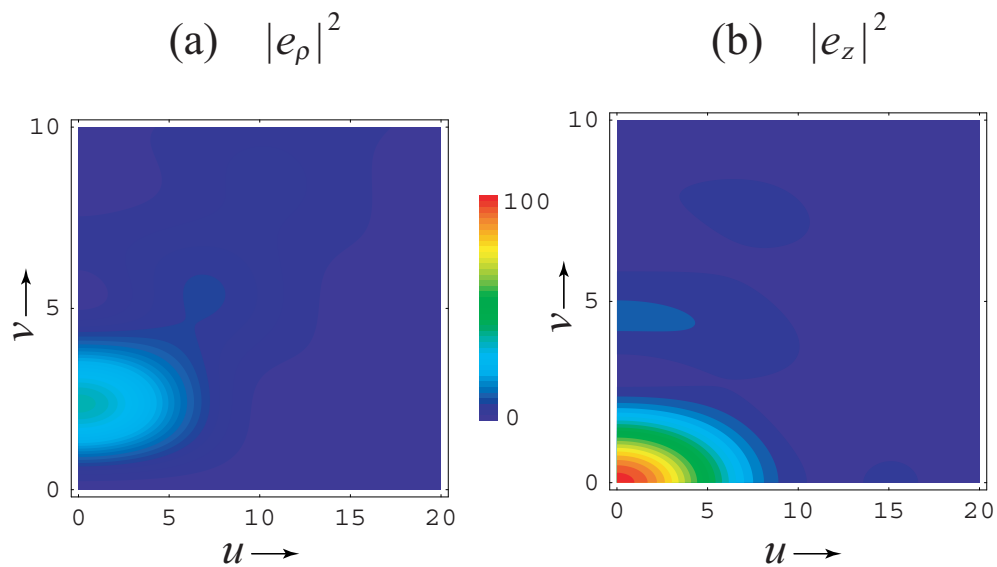


Figure 3.3: Contours of $|e_\rho(u, v)|^2$ (a) and $|e_z(u, v)|^2$ (b). In this example the semi-aperture angle $\alpha = \pi/3$, and the beam parameter $\beta = 0.6$.

3.4 Phase singularities of the field components

In a previous paper we showed that the longitudinal electric field component of strongly focused, linearly polarized beams exhibits phase singularities [DIEHL AND VISSER, 2004]. We also showed that these singularities can be created or annihilated when the semi-aperture angle of the focusing system is changed. We now examine the existence of phase singularities of the two field components of the electric field in the focal region of focused, radially polarized beams. The presence of singular points (i.e., points of zero amplitude) of e_z is readily seen from Figs. 3.4 and 3.5 in which the phase of the field component is indicated by color. At points where different colors meet the field amplitude is zero and, consequently, the phase of the field component is singular.

In the description of linearly polarized light there is only a single free parameter, namely the semi-aperture angle α [DIEHL AND VISSER, 2004]. However, in the model for radially polarized light, there is an additional free parameter, namely the beam parameter β [See Eqs. (3.8) and (3.9)]. One might therefore guess that there are two different mechanisms for the creation or annihilation of phase singularities, namely varying the semi-aperture angle α , and varying the beam parameter β . This is found to be indeed the case. In Figure/Movie 3.4 an example of annihilations of phase singularities of the longitudinal field component e_z caused by smoothly increasing the semi-aperture angle α is presented. For, for example, $\alpha \approx 51.7^\circ$ an annihilation event can be seen near $(u, v) = (22, 10)$.

In Figure/Movie 3.5, the behavior of the same field component for varying values of the beam size parameter β is shown. Again, several annihilation events can be observed.

The radial field component e_ρ also possesses phase singularities. In Figure/Movie 3.6 it is shown how an Airy ring-like singularity is created on the z -axis when the beam parameter β is varied. This is reminiscent of an experimental observation reported in [KARMAN *et al.*, 1998].

3.5 The state of polarization in the focal plane

It is seen from Eqs. (3.8) and (3.9) that in the focal plane ($u = 0$) the longitudinal electric field component $e_z(0, v)$ is purely imaginary, whereas the radial electric field component $e_\rho(0, v)$ is real-valued. Thus, for all points in the focal plane we can separate the real and imaginary part of the electric field and write

$$\mathbf{e}(0, v) = e_\rho(0, v)\hat{\boldsymbol{\rho}} + i \operatorname{Im}[e_z(0, v)]\hat{\mathbf{z}}, \quad (3.11)$$

with $\hat{\boldsymbol{\rho}}$ and $\hat{\mathbf{z}}$ unit vectors in the radial and the longitudinal direction, respectively, and Im denotes the imaginary part. Since $e_\rho(0, v)\hat{\boldsymbol{\rho}}$ and $e_z(0, v)\hat{\mathbf{z}}$ are perpendicular

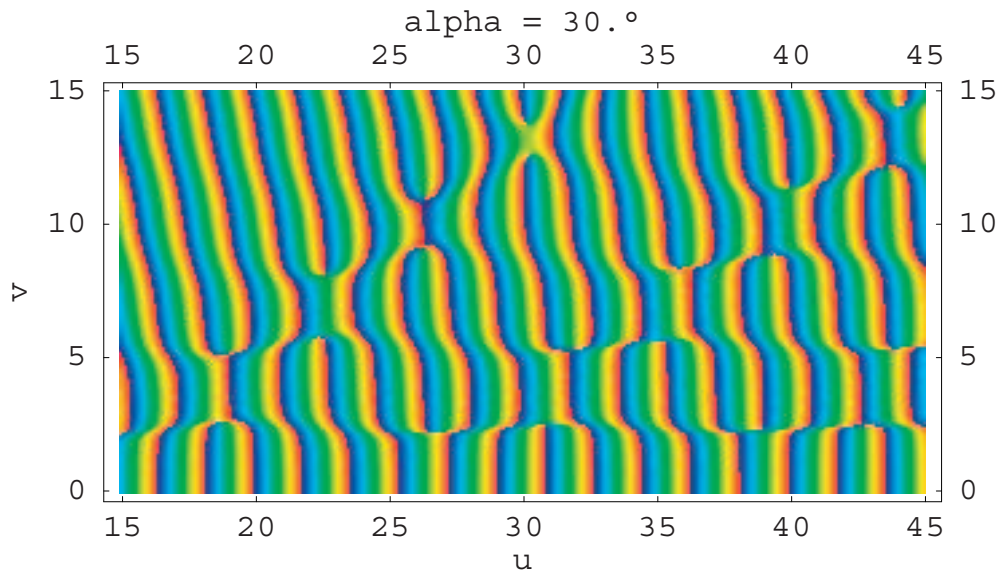


Figure 3.4: Color-coded plot of the phase of the longitudinal electric field component e_z for different values of the semi-aperture angle α . In this example $\beta = 0.6$.

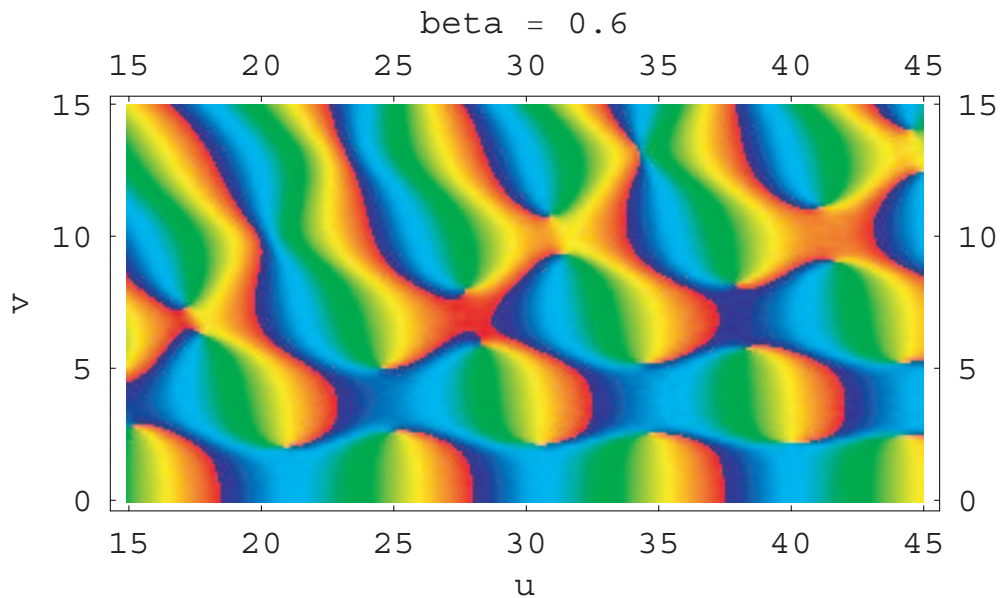


Figure 3.5: Color-coded plot of the phase of the longitudinal electric field component e_z for different values of the beam-size parameter β . In this example $\alpha = \pi/3$.

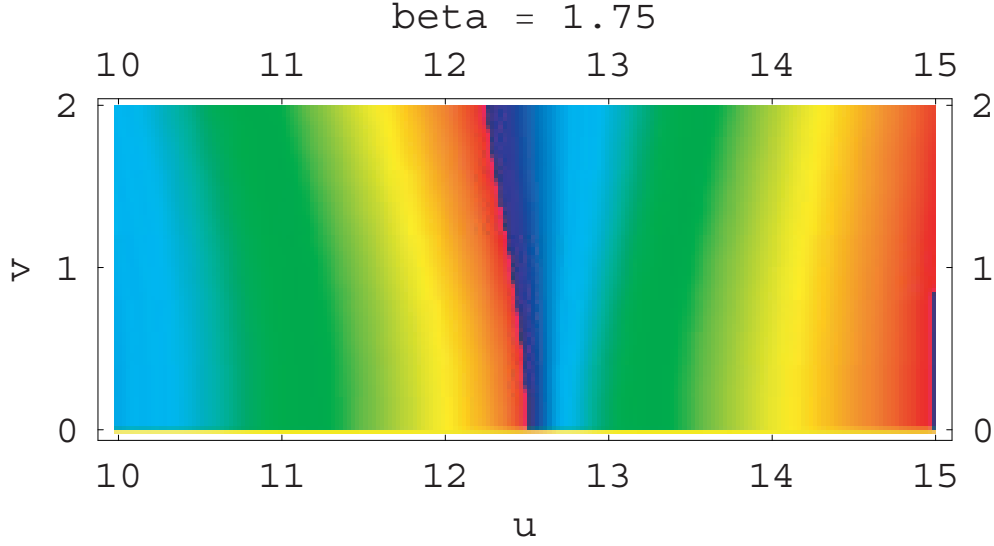


Figure 3.6: Color-coded plot of the phase of the radial electric field component e_ρ for different values of the beam-size parameter β . When β is decreased, an Airy ring-like singularity is created. In this example $\alpha = \pi/4$.

to each other, they constitute the conjugate semi-axes of the polarization ellipse. Moreover, $\hat{\rho}$ lies in the focal plane, whereas \hat{z} is perpendicular to it. Hence, *the polarization ellipse of the electric field at any point in the focal plane is at right angles to the focal plane*. Also, the plane of polarization (i.e., the plane formed by the polarization ellipse) at a point $(x, y, 0) = (v \cos \phi, v \sin \phi, 0)$ makes an angle ϕ with the xz -plane. The two axes of the polarization ellipse are in the ratio

$$R(v) = \frac{|\text{Im}[e_z(0, v)]|}{|e_\rho(0, v)|}. \quad (3.12)$$

The behavior of the two normalized electric field components $e_\rho(0, v)/\text{Im}[e_z(0, 0)]$ and $\text{Im}[e_z(0, v)]/\text{Im}[e_z(0, 0)]$ and the ratio $R(v)$ are both shown in Fig. 3.7. It is seen that at certain circles in the focal plane (e.g., $v = 3.0, 6.7$) the electric field is purely radial, whereas at others (e.g., $v = 0, 5.2$) the electric field is purely longitudinal. At the former points the field is linearly polarized along the radial direction with the ratio R being zero; at the latter points the field is linearly polarized along the z -direction with R being infinite. Both sets of circles constitute so-called *L-lines* in the focal plane [NYE, 1999]. We note that at points such as $v = 1.4, 4.4, 5.9$ where $R(v)$ equals unity (indicated by the dashed line in Fig. 3.7(b), the polarization is circular. In other words, the circles $v = 1.4, 4.4, 5.9$ form so-called *C-lines* in the focal plane.

The sense in which the electric polarization ellipse is traversed (i.e., its 'handed-

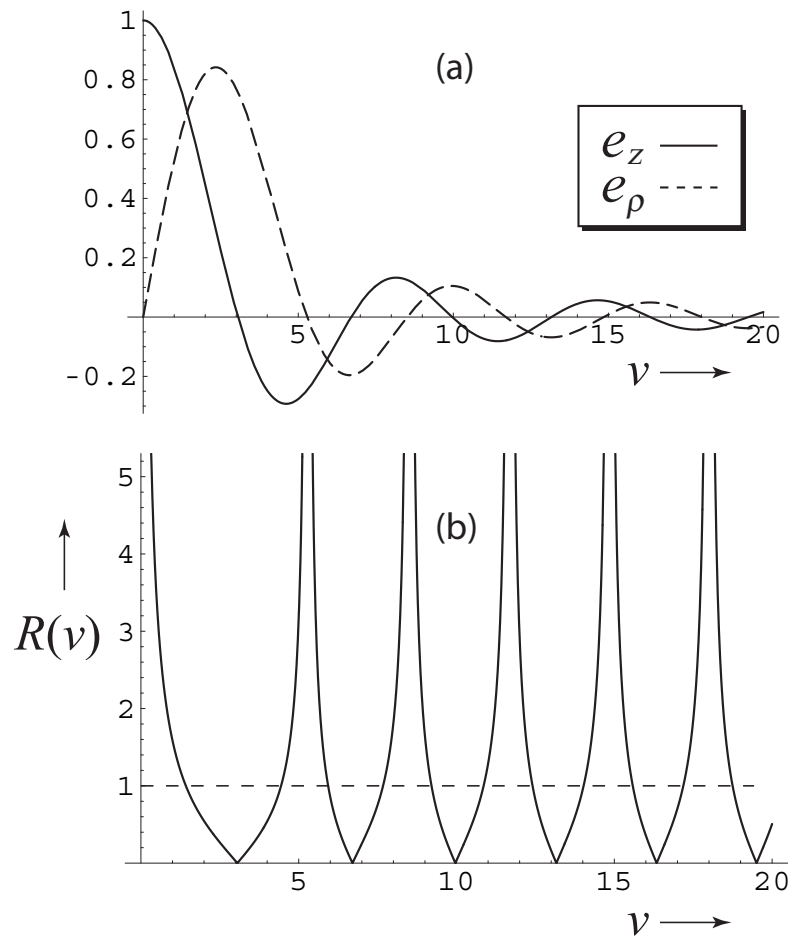


Figure 3.7: (a) Plot of the normalized electric field components $e_\rho(0, \nu)/\text{Im}[e_z(0, 0)]$ (dashed curve) and $\text{Im}[e_z(0, \nu)]/\text{Im}[e_z(0, 0)]$ (solid curve). (b) Plot of $R(\nu)$, the ratio of the lengths of the two conjugate semi-axes of the electric polarization ellipse. The different intersections with the horizontal dashed line (at which $R(\nu) = 1$) are points at which the polarization is circular. In this example the semi-aperture angle $\alpha = \pi/4$, and the beam parameter $\beta = 0.6$.

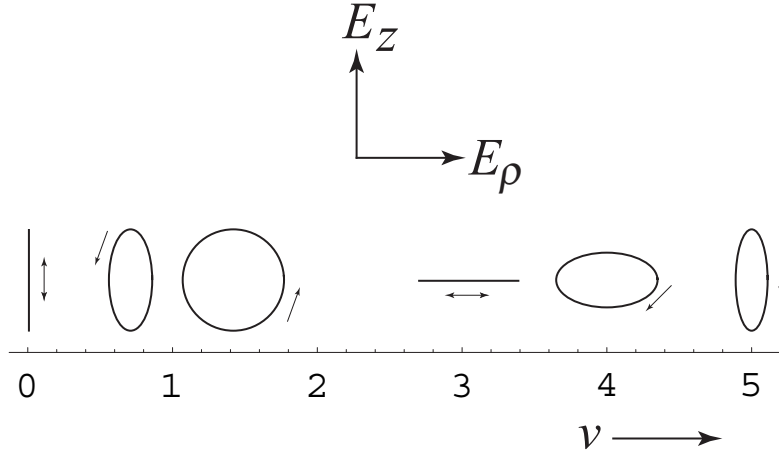


Figure 3.8: The electric polarization ellipse in the focal plane for selected values of the radial distance ($v = 0.00, 0.71, 1.42, 3.05, 4.00, 5.00$). The arrow indicates the direction in which the ellipse is being traversed. In this example the semi-aperture angle $\alpha = \pi/4$, and the beam parameter $\beta = 0.6$.

ness') can be determined by noting from Eqs. (3.1) and (3.11) that $\mathbf{E}(0, v, t = 0) = e_\rho(0, v)\hat{\boldsymbol{\rho}}$, whereas a quarter period later one has $\mathbf{E}(0, v, t = \pi/2\omega) = \text{Im}[e_z(0, v)]\hat{\mathbf{z}}$. This implies that if, on varying the radial distance v , one of the two electric field components changes sign, then so does the handedness of the state of polarization. Stated differently, *in the focal plane the L-lines (at which the polarization is linear) separate rings in which the electric polarization ellipse is being traversed in opposite directions*. The electric polarization ellipse and its handedness are shown in Fig. 3.8 for selected values of the radial position v . As a side remark we note, as can be seen from Fig. 3.7(a), that everywhere in the focal plane at least one of the two electric field components is non-zero. Hence, in contrast to focused linearly polarized fields [RICHARDS AND WOLF, 1959], nowhere in the focal plane does the total electric energy density (given by Eq. (3.10)) vanish.

3.6 The state of polarization in the focal region

The standard description of the state of polarization in terms of Stokes parameters [BORN AND WOLF, 1999] applies to plane waves, i.e. to fields in which the electric field only has two non-zero cartesian components, both perpendicular to the direction of propagation. On focusing a plane wave, the electric field acquires a third non-zero component which is directed along the direction of propagation (the so-called longitudinal field component) [RICHARDS AND WOLF, 1959]. Un-

der the assumption of paraxiality (i.e., assuming the semi-aperture angle of the focusing system to be small), this third component may be neglected. The configuration that we examine is not a paraxial one, but in cylindrical coordinates only two components of the electric field are non-zero. This means that with a suitable change in the definition of the Stokes parameters, the usual description of the state of polarization and, in particular, of polarization singularities [NYE, 1999] can be applied.

The electric field in the focal region is given by the formula

$$\mathbf{e}(u, v) = e_z(u, v)\hat{\mathbf{z}} + e_\rho(u, v)\hat{\boldsymbol{\rho}}, \quad (3.13)$$

with the components $e_z(u, v)$ and $e_\rho(u, v)$ given by Eqs. (3.8) and (3.9), and with $\hat{\mathbf{z}}$ and $\hat{\boldsymbol{\rho}}$ unit vectors in the longitudinal and radial direction, respectively. Let us define the variables

$$a_1 = |e_z(u, v)|, \quad (3.14)$$

$$\delta_1 = \arg[e_z(u, v)], \quad (3.15)$$

$$a_2 = |e_\rho(u, v)|, \quad (3.16)$$

$$\delta_2 = \arg[e_\rho(u, v)]. \quad (3.17)$$

The state of polarization of the field may then be characterized by the four Stokes parameters (cf. [BORN AND WOLF, 1999, Sec. 1.4] for a similar definition with respect to a cartesian coordinate system.)

$$S_0 = a_1^2 + a_2^2, \quad (3.18)$$

$$S_1 = a_1^2 - a_2^2, \quad (3.19)$$

$$S_2 = 2a_1a_2 \cos \delta, \quad (3.20)$$

$$S_3 = 2a_1a_2 \sin \delta, \quad (3.21)$$

with the phase difference δ given by

$$\delta = \delta_2 - \delta_1. \quad (3.22)$$

For any given intensity (i.e., $S_0 = \text{constant}$), the normalized Stokes parameters $s_1 = S_1/S_0$, $s_2 = S_2/S_0$ and $s_3 = S_3/S_0$ may be represented as a point on the Poincaré sphere (see Fig. 3.9). On the north pole ($s_1 = s_2 = 0, s_3 = 1$), the polarization is circular. We adopt the convention of calling this state right-handed because, according to Eq. (3.1), the ellipse is being traversed in a clockwise manner in the (e_z, e_ρ) -plane. The polarization is right-handed for points on the northern hemisphere, and left-handed for all points on the southern hemisphere. It easily verified that at the south pole ($s_1 = s_2 = 0, s_3 = -1$) the polarization is circular

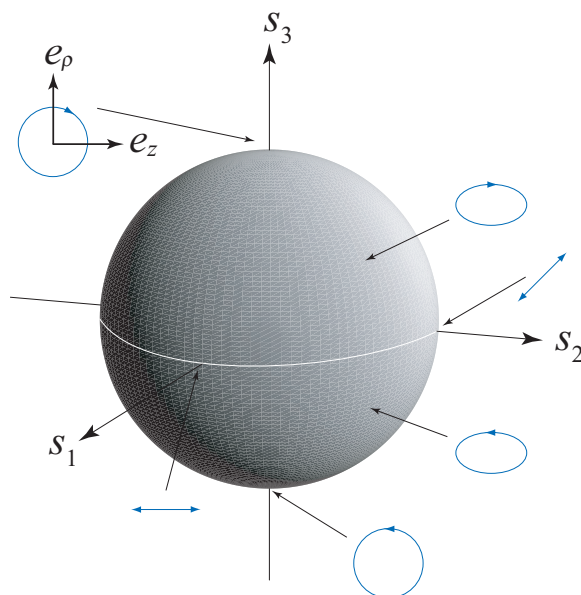


Figure 3.9: The Poincaré sphere with cartesian axes (s_1, s_2, s_3) .

and left-handed. For all points on the equator ($s_3 = 0$), the polarization is linear. At $(s_1 = 1, s_2 = s_3 = 0)$ the field is purely z -polarized, whereas at $(s_1 = -1, s_2 = s_3 = 0)$ it is purely ρ -polarized. At $(s_1 = 0, s_2 = 1, s_3 = 0)$ and $(s_1 = 0, s_2 = -1, s_3 = 0)$, finally, the linear polarization is under angle of $+\pi/4$ and $-\pi/4$ in the (e_z, e_ρ) -plane, respectively. For the case that $a_1 \geq a_2$, the orientation of the ellipse is described by the angle ψ between the major semiaxis and the z -direction. It is given by the expression [BORN AND WOLF, 1999, Sec. 1.4.2, Eq. (46)]

$$\psi = \frac{1}{2} \arctan \left(\frac{s_2}{s_1} \right). \quad (3.23)$$

It follows from Eqs. (3.8) and (3.9) that at any two points (u, v) and $(-u, v)$ that are symmetrically located with respect to the focal plane, the field components satisfy the symmetry relations

$$e_z(-u, v) = -e_z^*(u, v), \quad (3.24)$$

$$e_\rho(-u, v) = e_\rho^*(u, v), \quad (3.25)$$

where the asterisk denotes complex conjugation. Clearly, the two variables a_1 and a_2 remain unchanged under reflection of the point of observation in the focal plane. The behavior of the other quantities that describe the state of polarization under reflection of the point of observation in the focal plane is summarized in Table 1.

We note that the antisymmetrical behavior of the second Stokes parameter and the angle ψ implies that they both vanish identically in the focal plane, i.e.,

$$s_2(0, v) = 0; \quad \psi(0, v) = 0. \quad (3.26)$$

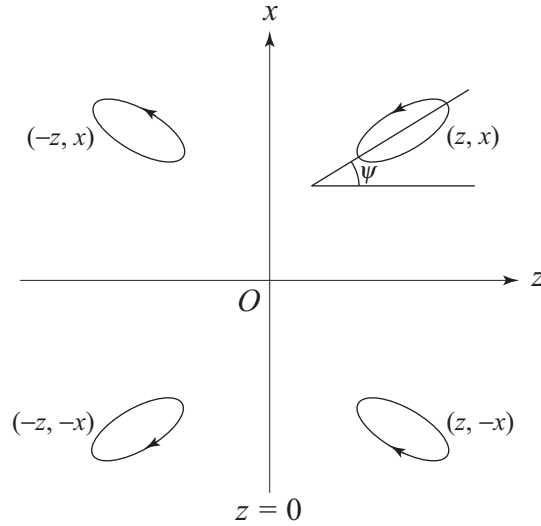


Figure 3.10: Illustrating the symmetry properties of the polarization ellipse.

The symmetry properties of the polarization ellipse are illustrated in Fig. 3.10. If, for example, the major semiaxis of the polarization ellipse at a point (z, x) makes an angle ψ with the positive z -axis, then at a point $(-z, x)$ the orientation angle will be $-\psi$. The handedness, however, will be the same at both positions. The orientation of the ellipse and its handedness at $(z, -x)$ and $(-z, -x)$ follow from considering the rotational symmetry of the field.

An example of the evolution of the Stokes parameters s_1 and s_3 in the focal plane as the radial distance v is increased is shown in Figure/Movie 3.11. Using the relation $s_1^2 + s_2^2 + s_3^2 = 1$ together with the first expression in (3.20), it is found

Table 3.1: The behavior of various quantities that characterize the state of polarization under reflection of the point of observation in the focal plane.

(u, v)	δ_1	δ_2	δ	s_0	s_1	s_2	s_3	ψ
$(-u, v)$	$\pi - \delta_1$	$-\delta_2$	$-\delta - \pi$	s_0	s_1	$-s_2$	s_3	$-\psi$

that for observation points in the focal plane the (s_1, s_3) vector has unit length. When the radial distance is increased, the state of polarization is seen to exhibit a cyclical behavior, changing from linear to circular and back to linear again. In other words, the Stokes vector traverses the $s_2 = 0$ meridian of the Poincaré sphere several times.

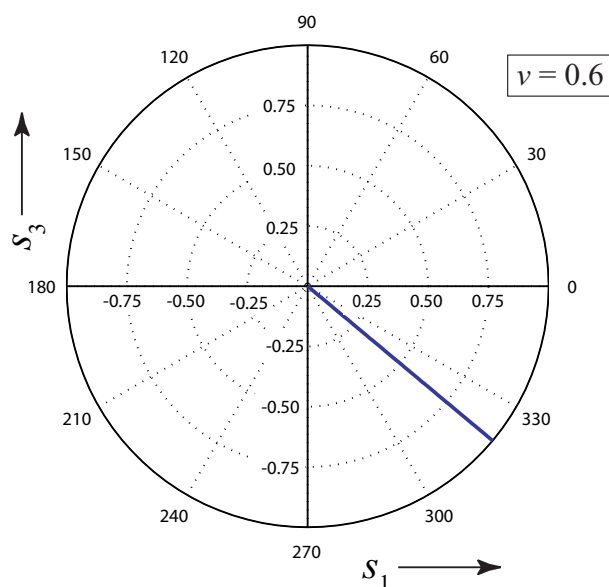


Figure 3.11: The normalized Stokes parameters s_1 and s_3 in the focal plane for increasing values of the dimensionless radial distance v . In this example $\alpha = \pi/4$ and $\beta = 1.5$.

3.7 Polarization singularities

At points where the polarization ellipse degenerates into a circle or into a line, the state of polarization is said to be singular. At C -points (i.e., $s_3 = \pm 1$), where the polarization is circular, the orientation angle ψ of the ellipse, as given by Eq. (3.23), is undetermined. At C -points the polarization can either be left-handed or right-handed. At L -lines (i.e., $s_3 = 0$), where the polarization is linear, the handedness of the ellipse is undetermined. In the remainder these two types of polarization singularities are examined. It should be noted that, because of

rotational symmetry, points and closed lines in the (u, v) -plane are circles and tori, respectively, in three-dimensional space.

3.7.1 Linear polarization

It follows from Eq. (3.21) that linear polarization generically occurs at points (u, v) at which

$$\operatorname{Re}[e_z(u, v)] \operatorname{Im}[e_\rho(u, v)] = \operatorname{Im}[e_z(u, v)] \operatorname{Re}[e_\rho(u, v)]. \quad (3.27)$$

This single condition is typically satisfied on a line in (u, v) -space. A subset of these points are locations where one of the two field components is zero, i.e. at phase singularities of either field component. For example, for the longitudinal component these occur at points at which

$$\operatorname{Re}[e_z(u, v)] = \operatorname{Im}[e_z(u, v)] = 0. \quad (3.28)$$

These two conditions are typically satisfied at isolated points in (u, v) -space. Phase singularities of both field components are found in the focal plane and at other points in space. They can be created or annihilated by smoothly varying the width of the incident beam or the semi-aperture angle [DIEHL *et al.*, 2006].

By drawing the contours of $s_3 = 0$, a multitude of L -surfaces is found. As is illustrated in Fig. 3.12, the phase singularities of the two electric field components all lie on L -surfaces. Notice that there is a surface of linear polarization that connects each Airy ring of e_z to the adjacent Airy ring of e_ρ . On traversing these closed surfaces in the focal plane, the Stokes vector makes a complete rotation along the equator of the Poincaré sphere.

It is seen from Eq. (3.9) that on the central axis (i.e., $v = 0$) the radial electric field component vanishes. Therefore this axis constitutes an L -line. It follows from rotational symmetry that its index is $+1$ (see [NYE, 1999, Sec. 13.3]).

3.7.2 Circular polarization

It is seen from the definitions (3.19)–(3.21) that circular polarization occurs generically at points in the u, v -plane. One way of locating them is to represent the field in a circular polarization basis (cf. [JACKSON, 1975] for an similar decomposition in cartesian coordinates), i.e.,

$$\mathbf{e}(u, v) = e_+(u, v)\hat{\mathbf{c}}_+(u, v) + e_-(u, v)\hat{\mathbf{c}}_-(u, v), \quad (3.29)$$

where

$$e_\pm = (e_z \mp ie_\rho)/\sqrt{2}, \quad \hat{\mathbf{c}}_\pm = (\hat{z} \pm i\hat{\rho})/\sqrt{2}. \quad (3.30)$$

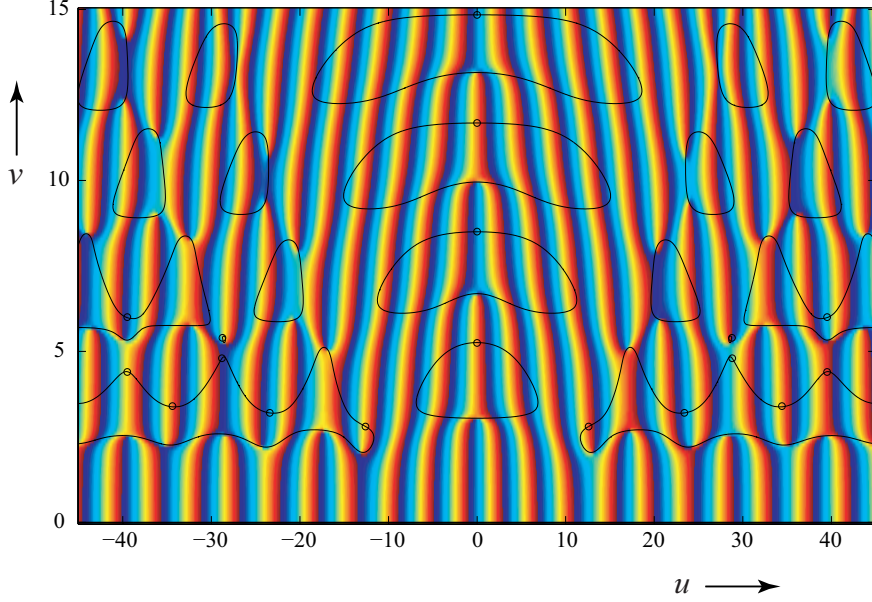


Figure 3.12: The loci of linear polarization, i.e. contours of $s_3 = 0$, in the focal region. Because of the rotational symmetry of the field, these are tori centered on the u -axis. The contours are superposed on a color-coded phase map of e_z . Phase singularities of e_z are located at points where all different colors converge. The open circles indicate phase singularities of the other field component, e_ρ . In this example $\alpha = \pi/4$ and $\beta = 0.5$.

Thus e_+ (e_-) represents the amplitude of the right- (left-) handed circular component of the field. In this way, C -points correspond to phase singularities of either component. An example is presented in Fig. 3.13. It is seen that the number of right- and left-handed C -points is approximately the same. However, there is a line (a cylindrical sheet in three-dimensional space) of left-handed circular polarization at approximately $v = 1.4$. This is a non-generic surface that appears to be only weakly dependent on the parameters u and β . To understand this feature more fully we apply a first-order Taylor expansion to Eqs. (3.8) and (3.9). These expressions then become

$$e_z(u, v) = -ikf^2 \int_0^\alpha \theta^3 \exp(-\beta^2 \theta^2) \exp(iu/\sin^2 \alpha) d\theta, \quad (3.31)$$

$$e_\rho(u, v) = -kf^2 \int_0^\alpha \theta^3 \exp(-\beta^2 \theta^2) \exp(iu/\sin^2 \alpha) \frac{v}{2 \sin \alpha} d\theta. \quad (3.32)$$

Thus, e_+ can be written as

$$e_+(u, v) = -ikf^2 \exp(iu/\sin^2 \alpha) \left[1 - \frac{v}{2 \sin \alpha} \right] \int_0^\alpha \theta^3 \exp(-\beta^2 \theta^2) d\theta. \quad (3.33)$$

It is readily apparent that left-handed circular polarization occurs when $v = 2 \sin \alpha$. Also, because the zero of e_+ is independent of the longitudinal variable u , this phase singularity is line-shaped. Notice that there is no corresponding C -surface for right-handed circular polarization because the resulting equation would yield (at first order) $v = -2 \sin \alpha$. To test the validity of this approximation, the computed location of the C -surface is compared to the approximate values in Table 2. Even when the semi-aperture angle $\alpha = 60^\circ$, the approximation holds quite well.

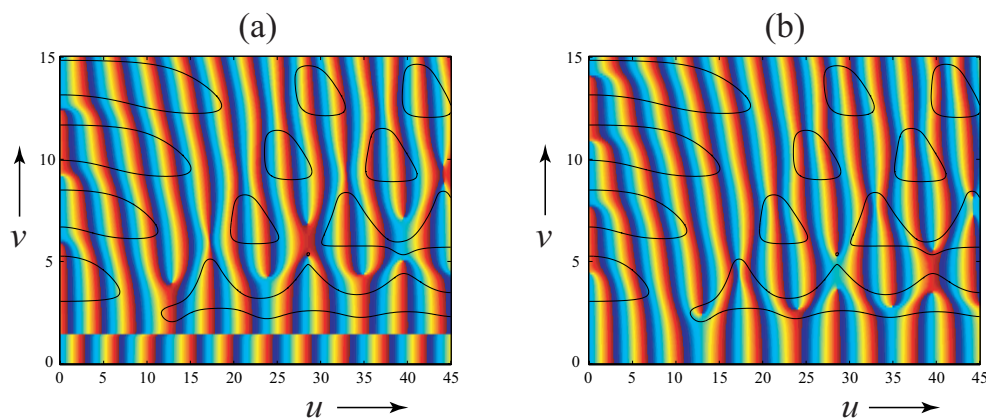


Figure 3.13: A color-coded phase map of (a) e_+ and (b) e_- , both with lines of linear polarization (solid black curves) superposed. Left-handed C -points are phase singularities of e_+ in panel (a), whereas right-handed C -points are singularities of e_- in panel (b). In this example $\beta = 0.5$ and $\alpha = \pi/4$.

Table 3.2: Comparison of the approximate location of the C -surface to its actual location. In these examples $\beta = 0.5$.

α	actual v	$v = 2 \sin \alpha$	Error
15°	0.515	0.517	0.50%
30°	1.005	1.000	0.50%
45°	1.425	1.414	0.76%
60°	1.765	1.732	1.87%

Apart from their handedness, C -points can be classified into three distinct types based on the local behavior of the polarization ellipses (see [NYE, 1999, Sec. 12.2]). These types are *stars* (with index $-1/2$), *monstars* (index $1/2$), and *lemons* (index $1/2$). This local behavior is shown in Fig. 3.14 for the pair of C -points seen in Fig. 3.13(b) near $(u, v) \approx (30, 5)$ for three different values of the semi-aperture angle α . Indicated in red are the local straight-line orientations of the major axis of the nearby ellipses. (A single line for a lemon, and three lines for stars and monstars). Notice that the lemon-type polarization singularity of Fig. 3.14(a) has evolved into a monstar in Fig. 3.14(b). In panel 3.14(c) the situation is shown after the star and the monstar have annihilated.

3.7.3 Relationship between L -lines and C -points

There is a strong connection between L -lines and C -points. The former separate space into regions of different handedness. In agreement with this, the left-handed C -points in Fig. 3.13(a), are all located outside the closed L -lines, whereas the right-handed C -points in Fig. 3.13(b) are all located within them. As reported by Freund et al. [FREUND *et al.*, 2002], there is a connection between the charge of component singularities on a closed L -line and the total charge of C -points enclosed by it. As is shown in Appendix A.1, for this specific case Eq. (5) of [FREUND *et al.*, 2002] can be re-written as

$$2 \sum_{\in L} q_- = \sum_L q_\rho + \sum_L q_z, \quad (3.34)$$

where the summation on the left-hand side is over all topological charges of C -points enclosed by the L -line, and the right-hand summations are over the charges of the two electric field components on the L -line. For example, it was verified that the two L -lines that contain the points $(0, 4)$ and $(22, 7)$ in Figs. 3.12 and 3.13 both satisfy this sum rule.

Figure/Movie 3.15 shows the evolution of the left-handed field component e_- and the L -lines as the semi-aperture angle α is increased. Notice that L -lines deform, separate, and merge. A small L -line that contains a C -point in its interior can be seen to break off when $\alpha \approx 43^\circ$, and unite with another L -line when $\alpha \approx 46.5^\circ$. In addition, a C -point annihilation is seen near $\alpha \approx 61^\circ$. The upper singularity is a star and the lower singularity is a lemon that evolves into a monstar before the annihilation takes place. Fig. 3.14 shows the corresponding local ellipse behavior for this event.

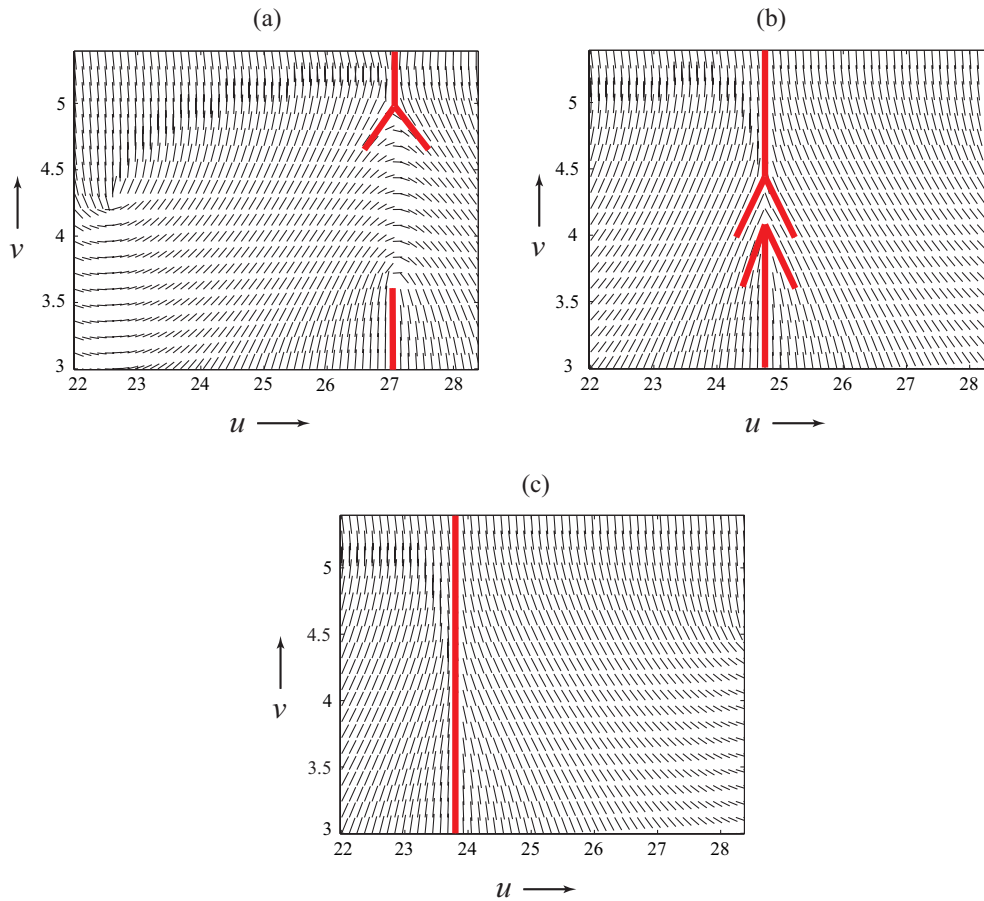


Figure 3.14: Local orientation of the major axis of the electric polarization ellipse shown for three different values of the semi-aperture angle α with the beam parameter β kept fixed at 0.5. The local straight-line orientation of the major axes are shown in red to aid the eye. In panel a ($\alpha = 52^\circ$), a star (above) and a lemon (below) are seen. In panel b ($\alpha = 61^\circ$), the lemon has transitioned into a monstar. In panel c ($\alpha = 65^\circ$), the annihilation leaves only a straight-line orientation of the major axis.

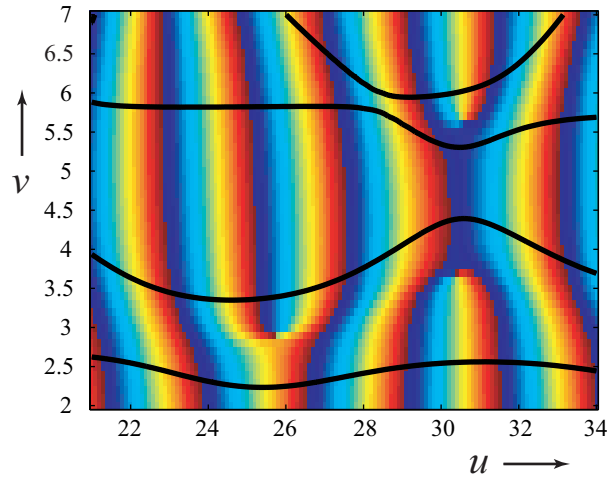


Figure 3.15: A color-coded phase map of the left-handed component e_- with L -lines, shown in black, superposed. The semi-aperture angle α is increased from 35° to 65.5° , with β kept fixed at 0.5.

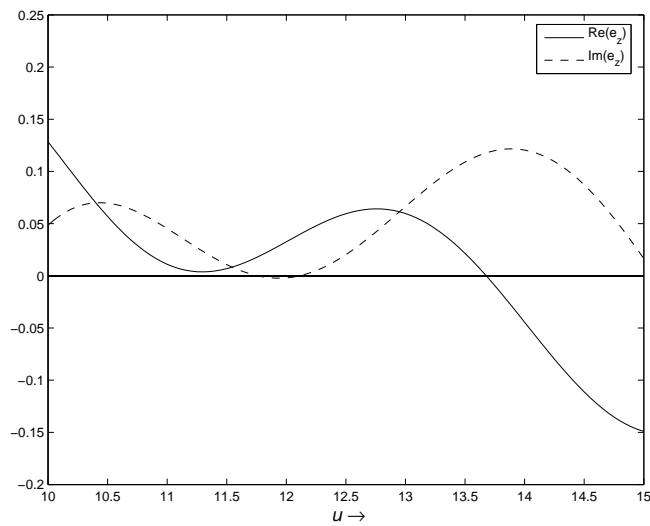


Figure 3.16: The real and imaginary parts of e_z along the optical axis normalized to $\text{Im}[e_z(0,0)]$ as α ranges from 55.0° to 58.0° , with β kept fixed at 1.5.

3.7.4 Vector singularities

In addition to the different kinds of singularities mentioned in Sec. 1, there exist also points where the two-dimensional complex electric vector field \mathbf{e} is identically zero. Such points are referred to as V -points [FREUND, 2002]. V -points are necessarily a phase singularity of both cartesian components and both components in the circular polarization basis. They are to be distinguished from singularities of real-valued vector fields such as the Poynting vector [SCHOUTEN *et al.*, 2003c; SCHOUTEN *et al.*, 2003b; SCHOUTEN *et al.*, 2004b]. Since the complex electric field given by Eqs. (3.8) and (3.9) is an analytic function, its zeros are isolated points in the (u, v) plane [COPSON, 1935]. Because the condition $\mathbf{e}(u, v) = 0$ has co-dimension four, V -points do not generically occur. However, as we now demonstrate, they do appear in the focal region of radially polarized beams.

In our configuration V -points occur, for example, when the longitudinal component e_z is zero on the optical axis (where the radial component e_ρ is identically zero). In Figure/Movie 3.16 the real and imaginary parts of e_z are shown. Their intersection near $u = 11.5$ is seen to move towards and eventually below the horizontal axis when the semi-aperture angle α is increased in a continuous manner. At approximately $\alpha = 56.6^\circ$, this intersection crosses the horizontal axis, i.e. $\text{Re}(e_z) = \text{Im}(e_z) = 0$ near $(u, v) = (11.5, 0)$. Clearly this V -point is unstable under perturbations.

Another way in which vector singularities may occur is through the collision of an L -line and a C -point [BERRY AND DENNIS, 2001]. Although the field at a V -point is neither linearly nor circularly polarized, the condition for linear polarization, ($S_3 = 0$) combined with the two conditions for circular polarization, ($S_1 = S_2 = 0$), result in the necessary condition that $S_0 = 0$, i.e. the electric field vanishes at the collision point. An example of such an event is shown in Figure/Movie 3.17 in which the semi-aperture angle α is gradually increased. The L -line that is seen to break apart moves downwards towards the horizontal C -line near $v = 1.6$. In this process the L -line shrinks and collapses to a point at the moment of collision. On further increasing α , this point changes back into an L -line that approaches the optical axis. The C -line remains essentially stationary while the L -line passes through it. We mention in passing that the L -line of interest in Figure/Movie 3.17 intersects one phase singularity of each cartesian component and encloses one point of pure right-handed circular polarization. When the L -line collapses to a point at the line of pure left-handed polarization (at approximately $v = 1.6$), both cartesian singularities coincide, creating a V -point. Alternatively, the V -point can be considered as the collision of phase singularities of the circular components e_+ and e_- . In fact, because L -surfaces separate space into regions of right- and left-handedness, the only way in which C -points of opposite

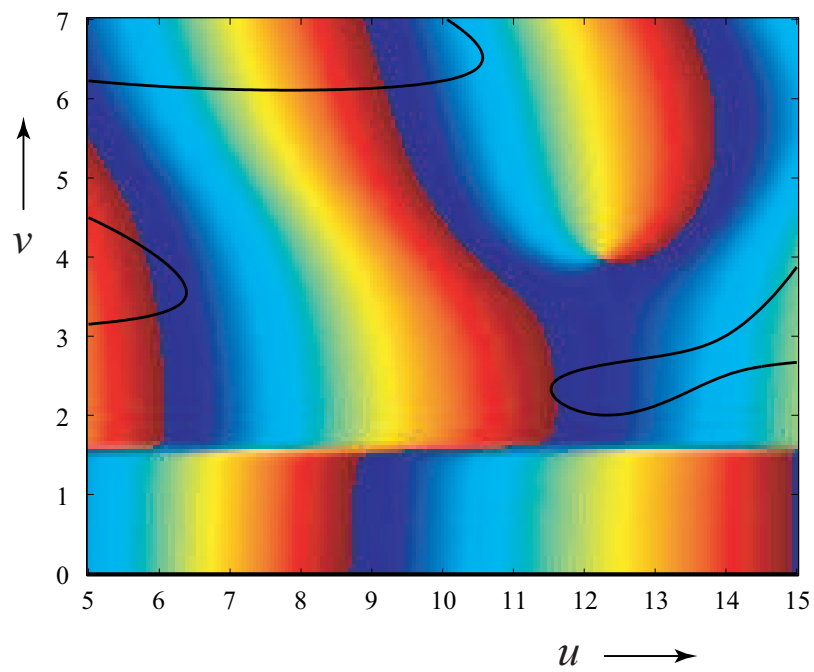


Figure 3.17: A color-coded phase map of e_+ with L -lines (solid black curves) superposed as the semi-aperture angle α ranges from 50.0° to 66.0° and with β kept fixed at 1.5.

handedness can collide is when the L -line separating them collapses to a point.

3.8 Discussion

It is to be noted that in the system at hand the magnetic field in the focal region has only a single (azimuthal) component. This implies that the behavior of the magnetic polarization is trivial compared to that of the electric polarization.

Also, because of the rotational symmetry of the configuration, the closed L -lines that are seen in the u, v -plane, form tori in three-dimensional space centered on the optical axis. Likewise, the C -points form rings.

In summary, strongly focused, radially polarized fields have been considered within the context of singular optics. The state of polarization was discussed and analyzed for this system. Phase singularities of the two electric field components and polarization singularities were identified. The relation between L -lines and C -lines was discussed, and an annihilation of two C -points involving a star, a lemon and a monstar, was shown. Finally, it was demonstrated that isolated vector singularities, V -points, can occur in this system and two different ways of creating them were analyzed.

Chapter 4

A Cascade of Singularities in Young's Interference Experiment

This Chapter is based on the following publication:

- T.D. Visser, **R.W. Schoonover**, “A cascade of singular field patterns in Young's interference experiment,” *Opt. Commun.* **281**, Issue 1, 1–6 (2008).

Abstract

We analyze Young's interference experiment for the case that two correlated, linearly polarized beams are used. It is shown that even when the incident fields are partially coherent, there are always correlation singularities (pairs of lines where the fields are completely uncorrelated) on the observation screen. These correlation singularities evolve in a non-trivial manner into dark lines (phase singularities in the paraxial approximation). The latter in turn each unfold into a triplet of polarization singularities, namely an L -line and two C -lines of opposite handedness.

4.1 Introduction

More than two centuries after its conception, Thomas Young's interference experiment [YOUNG, 1804; YOUNG, 1807; BORN AND WOLF, 1999] remains a source of novel insights. Several new effects have been predicted [SCHOUTEN *et al.*, 2003d; AGARWAL *et al.*, 2005] or observed [SCHOUTEN *et al.*, 2004a; KUZMIN *et al.*, 2007]. Also, so-called *correlation singularities* [FISCHER AND VISSER, 2004; PALACIOS *et al.*, 2004; SWARTZLANDER AND SCHMIT, 2004; WANG *et al.*, 2006], pairs of points at which the fields are completely uncorrelated, have been identified in Young's interference pattern [SCHOUTEN *et al.*, 2003a]. Several recent studies are concerned with the state of polarization of the field [MUJAT *et al.*, 2004; ROY-CHOWDHURY AND WOLF, 2005; SETALA *et al.*, 2006]. This aspect allows the study of a new kind of *singular behavior* [SOSKIN AND VASNETSOV, 2001]. Everywhere in a monochromatic field, the end-point of the electric vector traces out an ellipse over time. This polarization ellipse is characterized by three parameters describing its eccentricity, orientation and handedness. Polarization singularities [NYE, 1999; BERRY AND DENNIS, 2001; DENNIS, 2002; FREUND *et al.*, 2002; MOKHUN *et al.*, 2002; FREUND, 2002; SOSKIN *et al.*, 2003; SCHOONOVER AND VISSER, 2006], points where the ellipse has degenerated into a circle (so-called *C*-points, where the orientation of the ellipse is undefined) or into a line (so-called *L*-points, where the handedness is undefined), have, to the best of our knowledge, never been charted in the context of Young's experiment.

It has recently become apparent that different types of optical singularities are connected [GBUR *et al.*, 2004b]. In the present Chapter the relation between correlation singularities, dark lines, and polarization singularities is discussed. It is shown how each of them may occur in Young's double-slit experiment. Also, the continuous evolution of correlation singularities into dark lines and their subsequent unfolding into polarization singularities is described. This is done by analyzing the field that results from the superposition of two correlated beams with identical linear polarization. By gradually increasing the state of coherence of the two beams until they are fully coherent and co-phasal, pairs of correlation singularities are shown to transform into pairs of dark lines. If then the two directions of polarization are changed in a continuous manner from being parallel to making a finite angle with each other, each dark line is found to unfold into a pair of *C*-lines of opposite handedness plus an *L*-line. A possible experimental realization of this 'cascade' of field patterns is proposed.

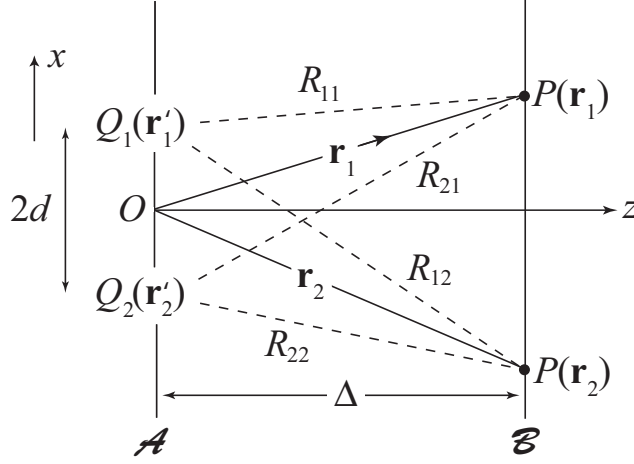


Figure 4.1: Illustrating the notation.

4.2 Correlation singularities and dark lines

Consider a plane, opaque screen \mathcal{A} with two identical, small apertures located at $Q_1(\mathbf{r}'_1)$ and $Q_2(\mathbf{r}'_2)$, that are separated by a distance $2d$ (see Fig. 4.1). At each aperture a linearly polarized beam is incident. The two beams are partially coherent, and their directions of polarization are for now taken to be parallel. The latter assumption allows us to use scalar diffraction theory. An interference pattern is formed on a second screen \mathcal{B} that is parallel to \mathcal{A} and a distance Δ away from it. Let

$$\mathbf{r}'_1 = (d, 0, 0) \quad \mathbf{r}'_2 = (-d, 0, 0), \quad (4.1)$$

and let the two incident fields at frequency ω be given by $U^{(\text{inc})}(\mathbf{r}'_1, \omega)$ and $U^{(\text{inc})}(\mathbf{r}'_2, \omega)$. The second-order coherence properties of the incident fields may be characterized by the *cross-spectral density function* [MANDEL AND WOLF, 1995], i.e.

$$W^{(\text{inc})}(\mathbf{r}'_1, \mathbf{r}'_2; \omega) = \langle U^{(\text{inc})*}(\mathbf{r}'_1, \omega) U^{(\text{inc})}(\mathbf{r}'_2, \omega) \rangle, \quad (4.2)$$

where the angle brackets denote averaging over an ensemble of field realizations. The *spectral degree of coherence* is the normalized version of the cross-spectral density function, viz.

$$\mu_{12}^{(\text{inc})}(\omega) = \frac{W^{(\text{inc})}(\mathbf{r}'_1, \mathbf{r}'_2; \omega)}{\sqrt{S^{(\text{inc})}(\mathbf{r}'_1, \omega) S^{(\text{inc})}(\mathbf{r}'_2, \omega)}}, \quad (4.3)$$

where

$$S^{(\text{inc})}(\mathbf{r}'_i, \omega) = W^{(\text{inc})}(\mathbf{r}'_i, \mathbf{r}'_i; \omega), \quad (i = 1, 2) \quad (4.4)$$

is the spectral density of the field at pinhole i . We assume the two spectral densities to be equal, i.e. $S^{(\text{inc})}(\mathbf{r}'_1, \omega) = S^{(\text{inc})}(\mathbf{r}'_2, \omega) = S^{(\text{inc})}(\omega)$.

It can be shown that the modulus of the spectral degree of coherence is bounded:

$$0 \leq |\mu_{12}^{(\text{inc})}(\omega)| \leq 1. \quad (4.5)$$

The lower bound corresponds to completely uncorrelated light, whereas the upper bound corresponds to fully coherent light. For all intermediate values the light is said to be partially coherent.

The field at two observation points $P(\mathbf{r}_1)$ and $P(\mathbf{r}_2)$ on screen \mathcal{B} is, assuming small angles of incidence and diffraction, given by the formulae [BORN AND WOLF, 1999, Sec. 8.8]

$$U(\mathbf{r}_1, \omega) = K_{11}U^{(\text{inc})}(\mathbf{r}'_1, \omega) + K_{21}U^{(\text{inc})}(\mathbf{r}'_2, \omega), \quad (4.6)$$

$$U(\mathbf{r}_2, \omega) = K_{12}U^{(\text{inc})}(\mathbf{r}'_1, \omega) + K_{22}U^{(\text{inc})}(\mathbf{r}'_2, \omega), \quad (4.7)$$

where

$$K_{ij} = -\frac{i}{\lambda}d\mathcal{A}\frac{e^{ikR_{ij}}}{R_{ij}}, \quad (i, j = 1, 2) \quad (4.8)$$

and $d\mathcal{A}$ denotes the area of each pinhole, R_{ij} the distance Q_iP_j and $k = 2\pi/\lambda = \omega/c$ is the wavenumber associated with frequency ω , λ being the wavelength and c the speed of light.

It is convenient to use the customary paraxial approximations [BORN AND WOLF, 1999, Sec. 8.8.1] for the factors K_{ij} , viz.

$$K_{1j} \approx -\frac{id\mathcal{A}}{\lambda R_{1j}}e^{ikR_{1j}}e^{-ik\mathbf{r}'_1 \cdot \hat{\mathbf{r}}_j} \approx -\frac{id\mathcal{A}}{\lambda\Delta}e^{ikR_{1j}}e^{-ikdx_j/\Delta}, \quad (4.9)$$

$$K_{2j} \approx -\frac{id\mathcal{A}}{\lambda R_{2j}}e^{ikR_{2j}}e^{-ik\mathbf{r}'_2 \cdot \hat{\mathbf{r}}_j} \approx -\frac{id\mathcal{A}}{\lambda\Delta}e^{ikR_{2j}}e^{ikdx_j/\Delta}, \quad (4.10)$$

where $\mathbf{r}_j = (x_j, y_j, z_j)$, $R_j = |\mathbf{r}_j|$ and $\hat{\mathbf{r}}_j = \mathbf{r}_j/R_j$. It is to be noted that the vector products appearing in Eqs. (4.9) and (4.10) imply that the observed field is, in the vicinity of the x -axis, essentially invariant in the direction perpendicular to the line connecting the two pinholes, i.e. in the y -direction. We will therefore restrict our analysis to observation points along the x -axis. It should be noted however, that the field behavior we discuss occurs along lines.

The cross-spectral density function of the field on screen \mathcal{B} is defined, strictly analogous to Eq. (4.2), as

$$W(\mathbf{r}_1, \mathbf{r}_2; \omega) = \langle U^*(\mathbf{r}_1, \omega)U(\mathbf{r}_2, \omega) \rangle, \quad (4.11)$$

with its spectral degree of coherence given by the expression

$$\mu(\mathbf{r}_1, \mathbf{r}_2; \omega) = \frac{W(\mathbf{r}_1, \mathbf{r}_2; \omega)}{\sqrt{S(\mathbf{r}_1, \omega)S(\mathbf{r}_2, \omega)}}, \quad (4.12)$$

where $S(\mathbf{r}_i, \omega) = W(\mathbf{r}_i, \mathbf{r}_i; \omega)$ is the spectral density at $P(\mathbf{r}_i)$. The modulus of the spectral degree of coherence of the field on the observation screen is again bounded, i.e.

$$0 \leq |\mu(\mathbf{r}_1, \mathbf{r}_2; \omega)| \leq 1, \quad (4.13)$$

with the bounds having the same meaning as for $\mu_{12}^{(\text{inc})}(\omega)$.

As mentioned before, we consider observation points that lie on the x -axis. As a further specialization, we will analyze pairs of points that are located symmetrically with respect to the z -axis, i.e. we take

$$\mathbf{r}_1 = (x, 0, \Delta), \quad (4.14)$$

$$\mathbf{r}_2 = (-x, 0, \Delta). \quad (4.15)$$

On substituting from Eqs. (4.6) and (4.7) into Eq. (4.11) while using the approximations (4.9) and (4.10) we then obtain for the spectral density and the cross-spectral density the expressions

$$S(\mathbf{r}_1, \omega) = 2 \left(\frac{dA}{\lambda \Delta} \right)^2 S^{(\text{inc})}(\omega) \left\{ 1 + |\mu_{12}^{(\text{inc})}(\omega)| \cos(\beta + 2kdx/\Delta) \right\} \quad (4.16)$$

$$S(\mathbf{r}_2, \omega) = 2 \left(\frac{dA}{\lambda \Delta} \right)^2 S^{(\text{inc})}(\omega) \left\{ 1 + |\mu_{12}^{(\text{inc})}(\omega)| \cos(\beta - 2kdx/\Delta) \right\} \quad (4.17)$$

$$W(\mathbf{r}_1, \mathbf{r}_2; \omega) = 2 \left(\frac{dA}{\lambda \Delta} \right)^2 S^{(\text{inc})}(\omega) \left\{ \text{Re}[\mu_{12}^{(\text{inc})}(\omega)] + \cos(2kdx/\Delta) \right\}, \quad (4.18)$$

where β denotes the argument (phase) of $\mu_{12}^{(\text{inc})}(\omega)$. We note that $S(\mathbf{r}_1, \omega) \neq S(\mathbf{r}_2, \omega)$ because, in general, $\mu_{12}^{(\text{inc})}(\omega) \neq \mu_{21}^{(\text{inc})}(\omega)$.

As is well known, there are no observation points where the spectral density vanishes when Young's experiment is performed using partially coherent light. (However, this is not necessarily true when *three* partially coherent beams are made to interfere. [GBUR *et al.*, 2004a; BASANO AND OTTONELLO, 2005; AMBROSINI *et al.*, 2005]) In the present case this follows from the fact that $|\mu_{12}^{(\text{inc})}(\omega)| < 1$ for partially coherent light, and therefore the terms in braces in Eqs. (4.16) and (4.17) have no zeros.

It is seen from Eqs. (4.16) and (4.17) that in the limit $\text{Re}[\mu_{12}^{(\text{inc})}(\omega)] \rightarrow 1$, i.e., when the two incident fields are fully coherent and co-phasal, the spectral density vanishes at points

$$\mathbf{r} = (x_n, 0, \Delta), \quad (4.19)$$

where

$$x_n = \pm \frac{\pi\Delta}{kd}(n + 1/2), \quad (n = 0, 1, 2, \dots) \quad (4.20)$$

It is to be noted that the complete destructive interference that leads to the spectral density to be zero at these points is a direct consequence of the use of the paraxial approximation [Eqs. (4.9) and (4.10)]. In reality, rather than phase singularities, there will be dark lines on the observation screen with a vanishing but non-zero intensity.

In contrast to the field amplitude, the behavior of the correlation functions is more subtle. There are pairs of observation points at which the fields are completely incoherent (i.e., pairs of points for which $W(\mathbf{r}_1, \mathbf{r}_2; \omega) = \mu(\mathbf{r}_1, \mathbf{r}_2; \omega) = 0$) even if the incident is partially coherent. A necessary and sufficient condition for this to occur is for the term in braces in Eq. (4.18) to become zero, i.e

$$\cos(2kdx/\Delta) = -\text{Re}[\mu_{12}^{(\text{inc})}(\omega)]. \quad (4.21)$$

In view of the relation (4.5) it follows that Eq. (4.21) can always be satisfied. So we conclude that *even if the two incident fields are partially coherent, there are pairs of observation points $\mathbf{r}_1 = (x, 0, \Delta)$, $\mathbf{r}_2 = (-x, 0, \Delta)$ at which the fields at frequency ω are completely uncorrelated.* Let us now examine the behavior of the solutions of Eq. (4.21) for the case that $\text{Re}[\mu_{12}^{(\text{inc})}(\omega)]$ is positive. We can write the positive solutions for the position x as

$$x_n^\pm = \frac{\pi\Delta}{kd}(\pm\delta + n + 1/2), \quad (n = 0, 1, 2, \dots), \quad (4.22)$$

with δ a positive constant that depends on the value of $\text{Re}[\mu_{12}^{(\text{inc})}(\omega)]$, and the superscript \pm indicating whether the plus or minus sign is taken in front of δ . If $\text{Re}[\mu_{12}^{(\text{inc})}(\omega)]$ tends to unity, δ becomes smaller and the points x_n^+ and x_n^- , that are each part of two different correlation singularities, namely the pairs of points $(-x_n^+, x_n^+)$ and $(-x_n^-, x_n^-)$, move closer to each other. In the limit of the two incident fields becoming fully coherent and co-phasal, the points x_n^+ and x_n^- merge and both correlation singularities disappear, i.e.

$$\lim_{\text{Re}[\mu_{12}^{(\text{inc})}(\omega)] \rightarrow 1} x_n^+ = x_n^- = x_n. \quad (4.23)$$

In this limit the points $\pm x_n^\pm$ become the dark lines given by Eq. (4.19). Hence we conclude that in the limit of the two incident fields becoming fully coherent and co-phasal (i.e., $\mu_{12}^{(\text{inc})}(\omega) = 1$), each half of the correlation singularity $(-x_n^+, x_n^+)$ annihilates with a neighboring half of the correlation singularity $(-x_n^-, x_n^-)$. The result of this 'cross-pair' annihilation of correlation singularities is a dark line at

x_n . (Only in the idealized paraxial case are these dark lines true zeros of intensity, i.e. phase singularities.)

An example is shown in Fig. 4.2 in which four coherence singularities (i.e. four pairs of points) are shown for selected values of the real part of the spectral degree of coherence, $\text{Re}[\mu_{12}^{(\text{inc})}(\omega)]$. In panel (a) the equally colored pairs $(-x_0^-, x_0^-)$, $(-x_0^+, x_0^+)$, $(-x_1^-, x_1^-)$ and $(-x_1^+, x_1^+)$ each form a coherence singularity, in other words $\mu(-x_0^-, x_0^-; \omega) = \mu(-x_0^+, x_0^+; \omega) = \mu(-x_1^-, x_1^-; \omega) = \mu(-x_1^+, x_1^+; \omega) = 0$. In panel (b) the same four coherence singularities are shown for a higher value of $\text{Re}[\mu_{12}^{(\text{inc})}(\omega)]$. It is seen that each half of a correlation singularity, like e.g. x_0^- , moves closer to a neighboring half of another correlation singularity, in this case x_0^+ . In panel (c) the limiting case of $\text{Re}[\mu_{12}^{(\text{inc})}(\omega)] = 1$ is shown. Now the four correlation singularities have annihilated, and four dark lines at $-x_1$, $-x_0$, x_0 , and x_1 have been created.

4.3 Dark lines and polarization singularities

In order to study polarization effects, we must use a vector description rather than the scalar description we used thus far. The incident fields are assumed to be fully coherent and linearly polarized. The two angles of polarization are under an angle α with each other. Let the electric fields at frequency ω that are incident on the two pinholes be given by the expressions

$$\mathbf{E}(\mathbf{r}'_1, \omega) = E \exp(-i\omega t) \hat{\mathbf{x}}, \quad (4.24)$$

$$\mathbf{E}(\mathbf{r}'_2, \omega) = E \exp(-i\omega t) [\cos \alpha \hat{\mathbf{x}} + \sin \alpha \hat{\mathbf{y}}], \quad (4.25)$$

where t denotes the time, and $\hat{\mathbf{x}}$ and $\hat{\mathbf{y}}$ are unit vectors in the x and y -direction, respectively, and $E \in \mathbb{R}$. The electric field at an observation point $P(\mathbf{r})$ is then, again assuming small angles of incidence and diffraction, given by the formula

$$\mathbf{E}(\mathbf{r}, \omega) = K_1 \mathbf{E}(\mathbf{r}'_1, \omega) + K_2 \mathbf{E}(\mathbf{r}'_2, \omega), \quad (4.26)$$

with

$$K_1 = -\frac{i}{\lambda} d\mathcal{A} \frac{e^{ik|\mathbf{r}-\mathbf{r}'_1|}}{|\mathbf{r}-\mathbf{r}'_1|} \approx -\frac{id\mathcal{A}}{\lambda\Delta} e^{ikR} e^{-ikdx/\Delta}, \quad (4.27)$$

$$K_2 = -\frac{i}{\lambda} d\mathcal{A} \frac{e^{ik|\mathbf{r}-\mathbf{r}'_2|}}{|\mathbf{r}-\mathbf{r}'_2|} \approx -\frac{id\mathcal{A}}{\lambda\Delta} e^{ikR} e^{ikdx/\Delta}, \quad (4.28)$$

where $\mathbf{r} = (x, y, \Delta)$, and $R = |\mathbf{r}|$. On substituting from Eqs. (4.24) and (4.25) into Eq. (4.26) while using the approximations (4.27) and (4.28), we obtain for the field on the screen the expression

$$\mathbf{E}(\mathbf{r}, \omega) = -i \frac{Ed\mathcal{A}}{\lambda\Delta} e^{i(kR-\omega t)} \left[(e^{-ikdx/\Delta} + \cos \alpha e^{ikdx/\Delta}) \hat{\mathbf{x}} + \sin \alpha e^{ikdx/\Delta} \hat{\mathbf{y}} \right]. \quad (4.29)$$

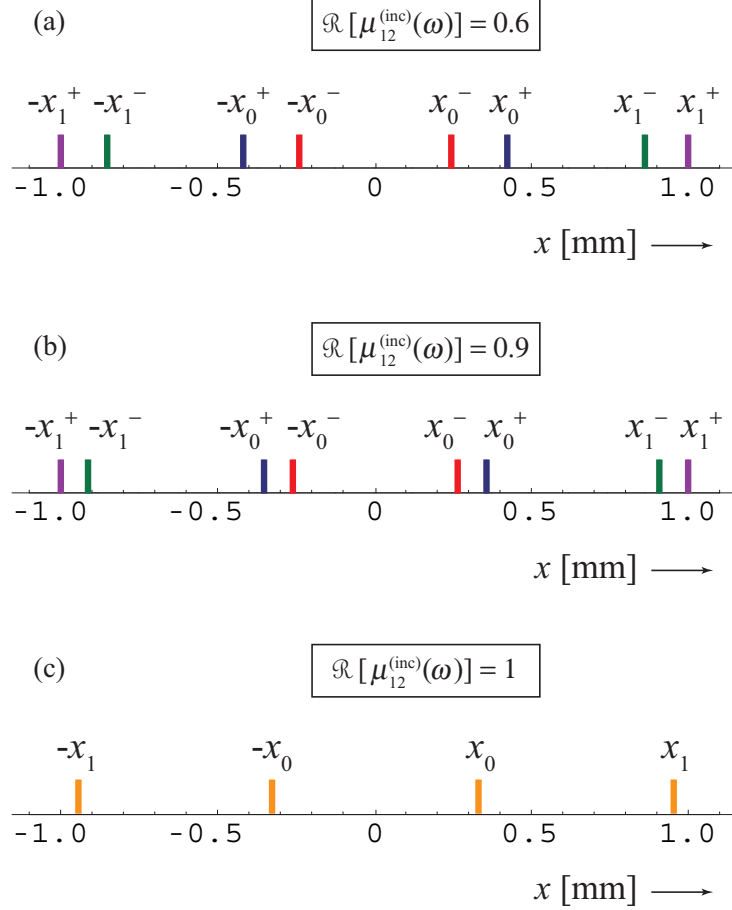


Figure 4.2: The position of four correlation singularities, i.e., the pairs of observation points $(-x_1^+, x_1^+)$, $(-x_1^-, x_1^-)$, $(-x_0^+, x_0^+)$, and $(-x_0^-, x_0^-)$ at which the fields are completely uncorrelated, for selected values of $\Re[\mu_{12}^{(\text{inc})}(\omega)]$. The pairs are indicated by equally-colored bars. In panels (a) and (b) it is seen how each half of a singularity moves towards a neighboring half. In panel (c) the incident fields are fully coherent and co-phasal. The four correlation singularities have annihilated and four dark lines have been created at $-x_1$, $-x_0$, x_0 , and x_1 . In this example $\lambda = 632.8$ nm, $\Delta = 2$ m, and $2d = 2$ mm.

If we define

$$a_1 = |E_x(\mathbf{r}, \omega)|, \quad a_2 = |E_y(\mathbf{r}, \omega)|, \quad (4.30)$$

$$\delta_1 = \arg E_x(\mathbf{r}, \omega), \quad \delta_2 = \arg E_y(\mathbf{r}, \omega), \quad (4.31)$$

then the Stokes parameters that characterize the state of polarization of the field at $P(\mathbf{r})$ can be expressed as [BORN AND WOLF, 1999]

$$S_0 = a_1^2 + a_2^2, \quad S_1 = a_1^2 - a_2^2, \quad (4.32)$$

$$S_2 = 2a_1a_2 \cos \delta, \quad S_3 = 2a_1a_2 \sin \delta, \quad (4.33)$$

where $\delta = \delta_2 - \delta_1$. The first parameter, S_0 , is proportional to the intensity of the field. The normalized Stokes vector (s_1, s_2, s_3) , with $s_i = S_i/S_0$ and $i = 1, 2, 3$, indicates a point on the Poincaré sphere. The north pole ($s_3 = 1$) and south pole ($s_3 = -1$) correspond to circular polarization. Points on the equator ($s_3 = 0$) correspond to linear polarization. All other points correspond to elliptical polarization. At points above the equator ($s_3 > 0$) the polarization is right-handed, whereas as at points below the equator ($s_3 < 0$) the polarization is left-handed. The smallest angle between the major axis of the polarization ellipse and the positive x -axis equals

$$\Psi = \frac{1}{2} \arctan \left(\frac{s_2}{s_1} \right). \quad (4.34)$$

Let us now study the behavior of the Stokes parameters in the vicinity of a dark line (with near-zero intensity) that occurs when the two directions of polarization are parallel, i.e. when $\alpha = 0$. In that case the field everywhere is linearly polarized along the x -direction ($s_1 = 1, s_2 = s_3 = 0$). This situation is depicted in Figs. 4.3(a) and (b). Also, according to Eqs. (4.32) and (4.29),

$$S_0 = \left[\frac{2Ed\mathcal{A}}{\lambda\Delta} \cos(kdx/\Delta) \right]^2. \quad (4.35)$$

Hence we find as before that (albeit it only in the paraxial approximation) the intensity vanishes at the points x_n given by Eq. (4.20). If we consider the field around the point x_0 and apply a Taylor expansion to Eq. (4.29) for small values of the angle α , we find that

$$E_x(x_0, \omega) = 0, \quad (4.36)$$

$$E_y(x_0, \omega) = i \frac{\alpha Ed\mathcal{A}}{\lambda\Delta}. \quad (4.37)$$

Hence, on changing α from zero to a finite value, the x -component of the electric field remains approximately zero, whereas the y -component obtains a finite imaginary value. Thus, the dark line at x_0 evolves into a polarization singularity, namely

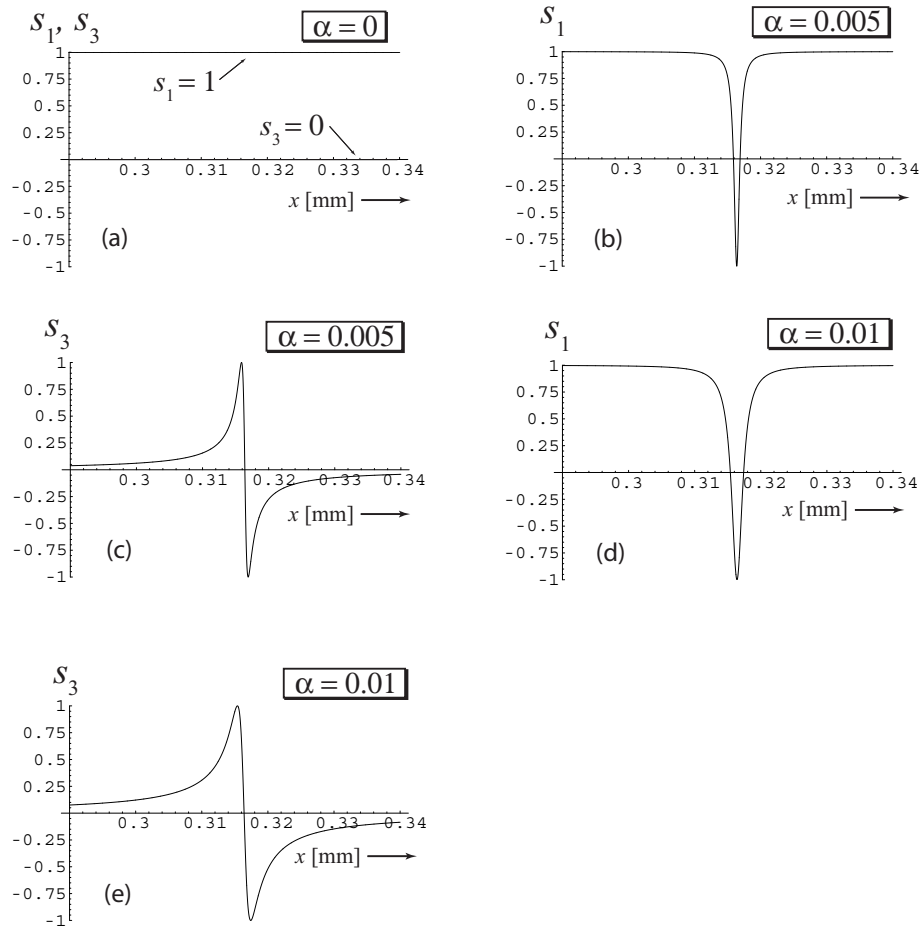


Figure 4.3: The Stokes parameters s_1 and s_3 as a function of position for selected values of the orientation angle α . In this example $\lambda = 632.8$ nm, $\Delta = 2$ m, and $2d = 2$ mm.

an L -line with $s_1 = -1$. We also note that the first term in the square brackets of Eq. (4.29) is approximately real near x_0 , whereas the second term is approximately imaginary. That implies that the Stokes parameter s_2 , remains unaffected, i.e. close to zero, under small changes in the angle α . To study the behavior of the parameter s_3 , it is useful to expand the electric field given by Eq. (4.29) in the circular polarization basis [JACKSON, 1975] as

$$e_{\pm}(\mathbf{r}, \omega) = -i \frac{E d \mathcal{A}}{\lambda \Delta \sqrt{2}} e^{i(kR - \omega t)} \left[e^{-ikdx/\Delta} + \cos \alpha e^{ikdx/\Delta} \mp i \sin \alpha e^{ikdx/\Delta} \right] \quad (4.38)$$

$$= -i \frac{E d \mathcal{A}}{\lambda \Delta \sqrt{2}} e^{i(kR - \omega t)} \left[e^{ikdx/\Delta} e^{\mp i\alpha} + e^{-ikdx/\Delta} \right], \quad (4.39)$$

where e_+ and e_- are the amplitudes for the left-handed and right-handed circular polarization basis, respectively. The zeros of these quantities occur when

$$kdx_{\pm}/\Delta \mp \alpha = -kdx_{\pm}/\Delta + \pi, \quad (4.40)$$

i.e. at positions

$$x_{\pm} = x_0 \pm \frac{\alpha \Delta}{2kd}. \quad (4.41)$$

From Eq. (4.41) it follows that two C -lines of opposite handedness are located symmetrically around x_0 . Thus we conclude that *on changing the polarization angle α from zero to a finite value, each dark line unfolds into a triplet of polarization singularities, namely an L -line with two C -lines of opposite handedness on either side.* It is to be noted that according to Eq. (4.41) the polarization singularities move away from each other when the angle α is increased, but they remain in existence. In other words, they are structurally stable. We emphasize that, since our system is approximately invariant along the y -direction, we are dealing with C -lines rather than the generically occurring C -points [BOGATYRYOVA *et al.*, 2003; SOSKIN *et al.*, 2004; BOGATYRYOVA *et al.*, 2004]. Also, this unfolding is reminiscent of a similar process in crystal optics [FLOSSMANN *et al.*, 2005; FLOSSMANN *et al.*, 2006].

An example of the unfolding process is shown in Fig. 4.3. There the behavior of the Stokes parameters s_1 and s_3 in the vicinity of the dark line at x_0 is depicted for selected values of the angle α . In calculating the plots the exact expressions for the factors K_j are used, rather than their approximate forms. In Figs. 4.3(a) and (b) the case of two perfectly aligned directions of polarization ($\alpha = 0$) is shown. It is seen that $s_1 = 1$ and $s_3 = 0$ over the entire range, i.e. the field is everywhere linearly polarized along the x -direction. Figs. 4.3(c) and (d) show the state of polarization when the two polarization directions are under an angle $\alpha = 0.005$ with each other. Precisely at the location of the vanished dark line (at

$x_0 = 0.316$ mm) an L -line with $s_1 \approx -1$ has appeared. Also, the behavior of the Stokes parameter s_3 has drastically changed: to the left of x_0 a right-handed C -line ($s_3 = 1$) has appeared, together with a left-handed C -line ($s_3 = -1$) to the right of x_0 . In Figs. 4.3(e) and (f) the same Stokes parameters are shown for a larger value of the angle α . It is seen that the triplet of polarization singularities still occurs, but with the two C -lines further separated from each other, as is suggested by Eq. (4.41). Also, the behavior of the parameters in the neighborhood of the former dark line has become smoother. In all numerical calculations it was found that $|s_2| < 0.01$.

The effects predicted in this paper can be produced, for example, by using a setup described by Thompson and Wolf [THOMPSON AND WOLF, 1957] that produces a field with a variable spectral degree of coherence. By adding two polarizers, the angle α between the two directions of polarization of the incident fields can be controlled.

4.4 Conclusions

An analysis of Young's interference experiment for the case when two correlated beams of identical linear polarization are used was presented. It was found that correlation singularities are always present. When the two beams become fully coherent and co-phasal, the correlation singularities annihilate in a cross-pair wise manner, and dark lines are created. On changing the polarization directions with respect to each other, each dark line unfolds into a triplet of polarization singularities.

Chapter 5

Polarization Singularities in an N -Pinhole Interferometer

This Chapter is based on the following publication:

- **R.W. Schoonover**, T.D. Visser, “Creating polarization singularities with an N -pinhole interferometer,” *Phys. Rev. A* **79**, 043809 (2009).

Abstract

Recent studies of singularities in scalar wave fields in Young’s classic experiment are extended to electromagnetic fields diffracted by an N -pinhole interferometer. Linearly polarized fields whose direction of polarization may be different at each pinhole are examined. It is shown that for two pinholes, only surfaces of linear polarization are created. For N larger than two, a rich structure of polarization singularities is found even when the location of the pinholes is arbitrary. In addition, there can be regions where the spectral density of the field is zero.

5.1 Introduction

Singular optics [NYE, 1999; SOSKIN AND VASNETSOV, 2001] is a relatively new branch of physical optics that analyzes topological features in the vicinity of singular points in wave fields. Originally it dealt with *phase singularities* and *polarization singularities* in monochromatic fields [BERRY AND DENNIS, 2001; DENNIS, 2002; FREUND *et al.*, 2002; MOKHUN *et al.*, 2002; SOSKIN *et al.*, 2003; SCHOONOVER AND VISSER, 2006]. Later it expanded to include spatially coherent, polychromatic fields in which *spectral anomalies* can occur [GBUR *et al.*, 2001]. More recently, *coherence singularities* in partially coherent fields have also been studied [FISCHER AND VISSER, 2004; PALACIOS *et al.*, 2004; SWARTZLANDER AND SCHMIT, 2004; WANG *et al.*, 2006; MALEEVA AND SWARTZLANDER, 2008; GBUR AND SWARTZLANDER, 2008].

Several studies have been dedicated to identifying different kinds of field singularities that can occur in Young's interference experiment. Phase singularities of the correlation function of the field resulting from the illumination of a multipinhole interferometer with a partially coherent field have been predicted [SCHOUTEN *et al.*, 2003a; GBUR *et al.*, 2004a; GAN AND GBUR, 2007] and observed [BASANO AND OTTONELLO, 2005; AMBROSINI *et al.*, 2005]. Optical vortices produced in a three-pinhole experiment with monochromatic scalar fields have also been analyzed [RUBEN AND PAGANIN, 2007]. Furthermore, the evolution of different types of singularities in a two-slit configuration – phase singularities of monochromatic scalar fields, coherence singularities of partially coherent scalar fields, and polarization singularities of vector fields – has recently been described [VISSER AND SCHOONOVER, 2008].

It is the aim of the present paper to elucidate the different types of polarization singularities that can occur in an N -pinhole experiment. Polarization singularities in monochromatic fields occur at positions (typically lines) where the polarization ellipse is circular and hence its orientation angle is undefined (C -lines), and at positions (typically surfaces) where the ellipse has degenerated into a line and therefore its handedness is undefined (L -surfaces) [NYE, 1999]. Often, these singular structures are examined in a specific plane, which leads to the identification of C -points and L -lines. We show that in the two-pinhole setup, with the field at each pinhole being linearly polarized, surfaces of linear polarization are created, but that circular polarization can only be created on, at most, a single surface. In the three-pinhole configuration, surfaces of linear polarization can be created, as can lines of circular polarization. These results are displayed only for planes perpendicular to the interferometer screen, resulting in lines and points rather than surfaces and lines. We show that for $N = 3$ a rich polarization topology occurs, even when the location of the pinholes lack symmetry. The extension to an N -pinhole setup is also discussed, and field structures for $N = 4$ and $N = 7$

are presented for symmetric pinhole configurations.

Our analysis does not only shed light on Young's interference experiment, one of the seminal experiments in physics, but it can also be applied to spatial control of the state of polarization. Having this capability is essential in Quantum Optics [LOUDON, 2003], but also in Classical Optics [BROSSEAU, 1998] where many components and samples [DAVIS AND CARNEY, 2008] are birefringent.

5.2 The two-pinhole interferometer

Consider an opaque screen occupying the plane $z = 0$ that is perforated by two identical pinholes. The pinholes are located at

$$\mathbf{r}_1 = (d, 0, 0), \quad \text{and} \quad \mathbf{r}_2 = (-d, 0, 0). \quad (5.1)$$

The field incident upon the pinholes is taken to be monochromatic with frequency ω , and linearly polarized. It is also assumed that the field at each pinhole is of equal amplitude and co-phasal. Let us write the electric field at the j -th pinhole as

$$\mathbf{E}_j(\omega) = E_0 e^{i\omega t} \hat{\mathbf{e}}_j, \quad (j = 1, 2) \quad (5.2)$$

where $E_0 \in \text{Re}$, t denotes the time and $\hat{\mathbf{e}}_j$ is a real unit vector that denotes the direction of polarization. The field at an observation point $\mathbf{r} = (x, y, z)$ then equals [BORN AND WOLF, 1999, Sec. 8.8]

$$\mathbf{E}(\mathbf{r}, \omega) = \bar{E}(\omega) \sum_{j=1}^2 \frac{e^{ikR_j}}{R_j} \hat{\mathbf{e}}_j, \quad (5.3)$$

where $R_j = |\mathbf{r} - \mathbf{r}_j|$, $\bar{E}(\omega) = -iE_0 d\mathcal{A} \exp(i\omega t)/\lambda$, $d\mathcal{A}$ is the area of each pinhole, and $k = \omega/c = 2\pi/\lambda$ is the wavenumber associated with frequency ω , c being the speed of light in vacuum. Obviously, if $\hat{\mathbf{e}}_1 \parallel \hat{\mathbf{e}}_2$, the resultant field will be linearly polarized everywhere. As is shown in the Appendix, all polarization choices except $\hat{\mathbf{e}}_1 \parallel \hat{\mathbf{e}}_2$ result in the same topological structure. We will therefore consider the case of two orthogonally polarized fields, namely $\hat{\mathbf{e}}_1 = \hat{\mathbf{x}}$ and $\hat{\mathbf{e}}_2 = \hat{\mathbf{y}}$. Using this choice in Eq. (5.3), and by denoting

$$|E_x(\mathbf{r}, \omega)| = E_0 d\mathcal{A} / \lambda R_1, \quad (5.4)$$

$$|E_y(\mathbf{r}, \omega)| = E_0 d\mathcal{A} / \lambda R_2, \quad (5.5)$$

$$\begin{aligned} \delta &= \arg [E_y(\mathbf{r}, \omega)] - \arg [E_x(\mathbf{r}, \omega)], \\ &= k(R_2 - R_1), \end{aligned} \quad (5.6)$$

the Stokes parameters that characterize the state of polarization of the field at position \mathbf{r} can be expressed as [BORN AND WOLF, 1999, Sec. 1.4.2]

$$S_0(\mathbf{r}, \omega) = |E_x(\mathbf{r}, \omega)|^2 + |E_y(\mathbf{r}, \omega)|^2, \quad (5.7)$$

$$S_1(\mathbf{r}, \omega) = |E_x(\mathbf{r}, \omega)|^2 - |E_y(\mathbf{r}, \omega)|^2, \quad (5.8)$$

$$S_2(\mathbf{r}, \omega) = 2 \operatorname{Re}\{E_x^*(\mathbf{r}, \omega)E_y(\mathbf{r}, \omega)\}, \quad (5.9)$$

$$S_3(\mathbf{r}, \omega) = 2 \operatorname{Im}\{E_x^*(\mathbf{r}, \omega)E_y(\mathbf{r}, \omega)\}. \quad (5.10)$$

The parameter $S_0(\mathbf{r}, \omega)$ is proportional to the spectral density (or 'intensity at frequency ω ') of the field. The normalized Stokes vector (s_1, s_2, s_3) , with $s_i = S_i/S_0$ and $i = 1, 2, 3$ indicates a point on the Poincaré sphere. The North Pole ($s_3 = 1$) and South Pole ($s_3 = -1$) both correspond to circular polarization. Points on the Equator ($s_3 = 0$) correspond to linear polarization. All other points correspond to elliptical polarization. The orientation of the polarization ellipse also follows from the Stokes parameters.

Linear polarization occurs at positions where $s_3 = 0$. This implies that

$$\delta = k(R_2 - R_1) = n\pi, \quad (5.11)$$

with n an integer. Substitution of the definitions of R_1 and R_2 results in the equation

$$\frac{x^2}{a_n^2} - \frac{y^2}{b_n^2} - \frac{z^2}{b_n^2} = 1, \quad (5.12)$$

where

$$a_n^2 = n^2\lambda^2/16, \quad (5.13)$$

$$b_n^2 = d^2 - a_n^2, \quad (n = 1, 2, \dots, n_{\max}). \quad (5.14)$$

Since $|R_2 - R_1| < 2d$ it follows that

$$n_{\max} < 4d/\lambda \leq n_{\max} + 1, \quad (5.15)$$

and hence the coefficients b_n^2 are all positive. Equation (5.12) represents a set of n_{\max} semi-hyperboloids of two sheets in the half-space $z > 0$, with their symmetry axis along the line connecting the two pinholes. The distance between the two x -intercepts of each hyperbola equals $2a_n = n\lambda/2$. These intercepts all lie in between the two pinholes. An example of the first two hyperbolas ($n = 1, 2$) is shown in Figs. 5.1 and 5.2. Putting $n = 0$ in Eq. (5.11) yields an additional surface on which the field is linearly polarized, namely the plane $x = 0$.

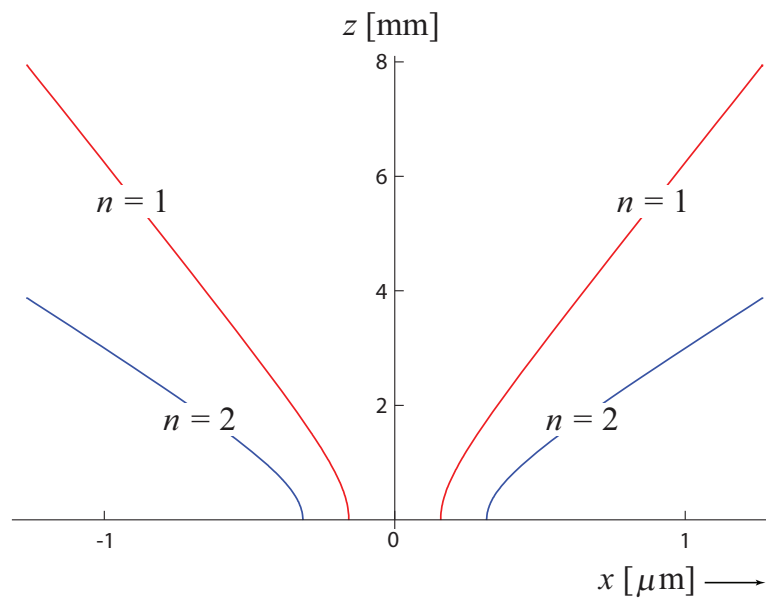


Figure 5.1: Semi-hyperbolas on which the polarization of the field in a two-pinhole interferometer is linear (L -surfaces). In this example $\lambda = 632.8$ nm and $2d = 2$ mm. Notice that the horizontal scale is in microns, whereas the vertical scale is in millimeters.

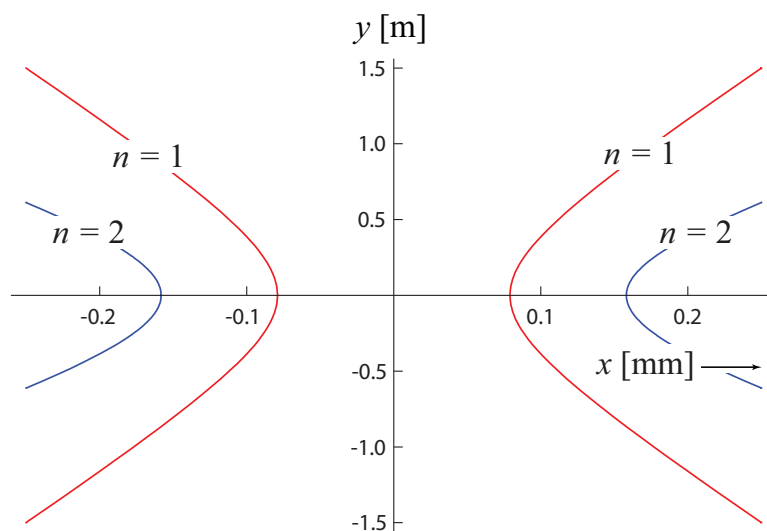


Figure 5.2: Semi-hyperbolas on which the polarization of the field in a two-pinhole interferometer is linear (L -surfaces). In this example $z = 0.5$ m. All other parameters are as in Fig. 5.1. Notice that the horizontal scale is in millimeters, whereas the vertical scale is in meters.

Circular polarization occurs at positions where both $s_1 = 0$ and $s_2 = 0$. The first condition implies that $R_1 = R_2$, *i.e.*, $x = 0$. From the second condition it follows that

$$\delta = k(R_2 - R_1) = (m + 1/2)\pi, \quad (5.16)$$

with m an integer. Substitution of the definitions of R_1 and R_2 results in the equation

$$\frac{x^2}{c_m^2} - \frac{y^2}{d_m^2} - \frac{z^2}{d_m^2} = 1, \quad (5.17)$$

where

$$c_m^2 = \left(m + \frac{1}{2}\right)^2 \lambda^2 / 16, \quad (5.18)$$

$$d_m^2 = d^2 - c_m^2, \quad (m = 0, 1, \dots, m_{\max}), \quad (5.19)$$

with

$$m_{\max} < \frac{4d}{\lambda} - \frac{1}{2} \leq m_{\max} + 1, \quad (5.20)$$

and the coefficients d_m^2 therefore all positive. Equation (5.17) represents a set of $m_{\max} + 1$ semi-hyperboloids of two sheets in the half-space $z > 0$, with their symmetry axis along the line connecting the two pinholes. The distance between the two x -intercepts of each hyperbola equals $2c_m = (m + 1/2)\lambda/2$. These intercepts too all lie in between the two pinholes. Since the surfaces of Eq. (5.17) and the plane $x = 0$ do not intersect, the two conditions for circular polarization cannot be satisfied simultaneously and so there is no location at which the field is circularly polarized. It is shown in the Appendix A.2 that under more general conditions than discussed here, C -points can occur in a $N = 2$ configuration.

5.3 The three-pinhole interferometer

An example of a symmetric three-pinhole interferometer configuration is one in which the pinholes are located at the vertices of an equilateral triangle with sides $\sqrt{3}d$:

$$\mathbf{r}_1 = d(0, 1, 0), \quad \mathbf{r}_2 = d\left(\frac{-\sqrt{3}}{2}, \frac{-1}{2}, 0\right), \quad \mathbf{r}_3 = d\left(\frac{\sqrt{3}}{2}, \frac{-1}{2}, 0\right). \quad (5.21)$$

The field at each pinhole is taken to have amplitude E_0 and to be linearly polarized along the radial direction, *i.e.*, $\hat{\mathbf{e}}_j = \hat{\mathbf{r}}_j$. This may be achieved, for example, by illuminating the screen with a radially polarized beam that propagates along the z -axis [YOUNGWORTH AND BROWN, 2000]. In the region of superposition the field is given by

$$\mathbf{E}(\mathbf{r}, \omega) = \bar{E}(\omega) \sum_{j=1}^3 \frac{e^{ikR_j}}{R_j} \hat{\mathbf{e}}_j. \quad (5.22)$$

By inserting Eq. (5.22) into Eqs. (5.10), one may again analyze the Stokes parameters of the field in an observation plane. In Fig. 5.3, the color-coded spectral density is shown in the transverse plane $z = 1$ m, with contours of $s_3 = 0$ (lines of linear polarization) superposed. A honeycomb pattern with many locations of near-zero spectral density is clearly visible. We also note that the line $x = y = 0$ is a so-called V -line, a line on which the total electric field is identically zero [NYE, 1999]. Both observations are a consequence of the particular choice of the pinhole positions. The appearance of a V -line is reminiscent of the complete destructive interference of partially coherent, scalar fields that has been predicted and observed for the same configuration [GBUR *et al.*, 2004a; BASANO AND OTTONELLO, 2005; AMBROSINI *et al.*, 2005].

There are three distinct sets of parallel L -lines in the plane shown in Fig. 5.3. This structure may be understood as follows. If we apply the paraxial approximation

$$e^{ikR_j}/R_j \approx e^{ikr} e^{-ik\hat{\mathbf{r}}\cdot\mathbf{r}_j}/r, \quad (5.23)$$

where $r = |\mathbf{r}|$ in Eq. (5.22), then the Stokes parameter $S_3(\mathbf{r}, \omega)$ is given by the expression

$$S_3(\mathbf{r}, \omega) = \frac{\sqrt{3}|\bar{E}(\omega)|^2}{r^2} \{ \sin[k\hat{\mathbf{r}} \cdot (\mathbf{r}_1 - \mathbf{r}_2)] + \sin[k\hat{\mathbf{r}} \cdot (\mathbf{r}_2 - \mathbf{r}_3)] + \sin[k\hat{\mathbf{r}} \cdot (\mathbf{r}_3 - \mathbf{r}_1)] \}. \quad (5.24)$$

By using the identity $\sin u + \sin v = 2 \cos[(u-v)/2] \sin[(u+v)/2]$ together with the relation $\mathbf{r}_1 + \mathbf{r}_2 + \mathbf{r}_3 = 0$, the first two terms on the right-hand side of Eq. (5.24) can be combined to give

$$S_3(\mathbf{r}, \omega) = \frac{\sqrt{3}|\bar{E}(\omega)|^2}{r^2} \{ -2 \cos(3k\hat{\mathbf{r}} \cdot \mathbf{r}_2/2) \sin[k\hat{\mathbf{r}} \cdot (\mathbf{r}_3 - \mathbf{r}_1)/2] + \sin[k\hat{\mathbf{r}} \cdot (\mathbf{r}_3 - \mathbf{r}_1)] \}. \quad (5.25)$$

In this case, $S_3(\mathbf{r}, \omega)$ vanishes when $k\hat{\mathbf{r}} \cdot (\mathbf{r}_3 - \mathbf{r}_1)/2$ is a multiple of π . Any two of the three sine terms in Eq. (5.24) can be combined to simplify the equation, and the condition $S_3(\mathbf{r}, \omega) = 0$ can thus be generalized to

$$\hat{\mathbf{r}} \cdot (\mathbf{r}_i - \mathbf{r}_j) = p\lambda \quad (i, j = 1, 2, 3 \text{ and } i \neq j), \quad (5.26)$$

with p an integer. For each value of p this gives us 3 equations that approximate lines in a transverse observation plane $z = z_0$. Consider first the case $i = 2, j = 3$, for which $\mathbf{r}_i - \mathbf{r}_j = s\hat{\mathbf{x}}$, with $s = -\sqrt{3}d$. Inserting this into Eq. (5.26) yields the condition

$$x_p^2 \left(1 - \frac{p^2\lambda^2}{s^2} \right) = \frac{p^2\lambda^2}{s^2} (y_p^2 + z_0^2), \quad (5.27)$$

where x_p and y_p are the locations of the p^{th} L -line in the plane $z = z_0$. The number of L -lines is bounded since $|p| \leq s/\lambda$. For $z_0 = 1 \text{ m} \gg y_p$, and taking $d = 1 \text{ mm}$, $\lambda = 0.6328 \mu\text{m}$, Eq. (5.27) reduces to

$$x_p \approx p 0.365 \text{ mm}, \quad (5.28)$$

the solutions of which correspond to the equidistant vertical L -lines. On setting $i = 1, j = 3$ in Eq. (5.26), a similar derivation yields

$$y_0 \approx \frac{x_0}{\sqrt{3}} + p 0.422 \text{ mm}. \quad (5.29)$$

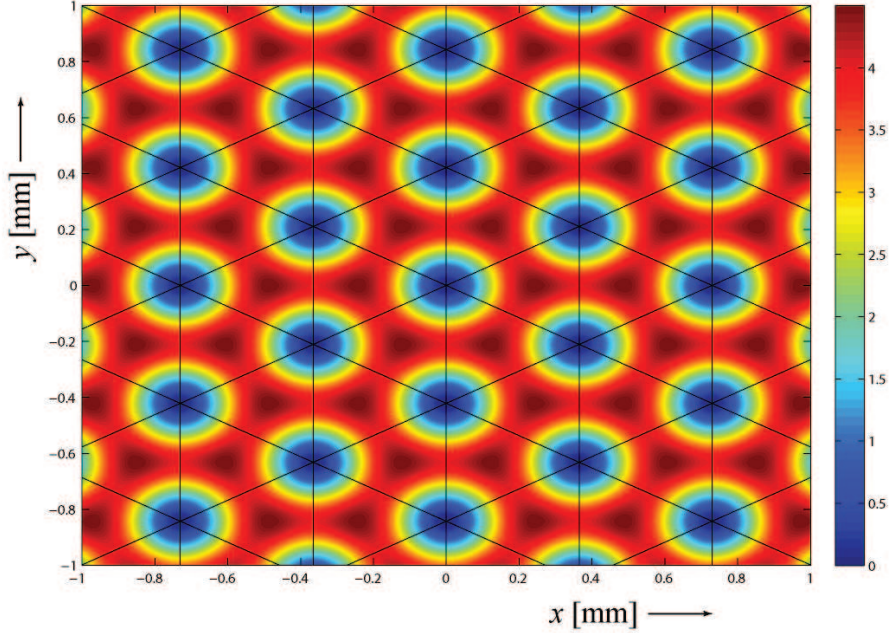


Figure 5.3: The spectral density (in arbitrary units) for the symmetric three-pinhole interferometer in the $z = 1$ m plane. The solid black curves are lines of linear polarization. In this example $d = 1$ mm and $\lambda = 632.8$ nm.

This expression describes the parallel L -lines that run from the bottom left corner to the top right corner in Fig. 5.3. It is easily verified that by setting $i = 1$, $j = 2$ in Eq. (5.26) one obtains the approximation

$$y_0 \approx -\frac{x_0}{\sqrt{3}} + p 0.422 \text{ mm}, \quad (5.30)$$

which corresponds to the remaining set of L -lines.

Unlike the two-pinhole case, circular polarization states do exist in the three-pinhole configuration. Right(Left)-handed circular polarization may be thought of as the condition when the field amplitude in the left(right)-handed polarization basis state vanishes. The electric field amplitudes for any two orthogonal basis states are generally complex, and so the location of phase singularities of the right(left)-handed amplitudes correspond to states of complete left(right)-handed polarization. By decomposing the field as [JACKSON, 1975, Sec. 7.2]

$$\mathbf{E}(\mathbf{r}, \omega) = E_+(\mathbf{r}, \omega)\hat{\mathbf{c}}_+ + E_-(\mathbf{r}, \omega)\hat{\mathbf{c}}_-, \quad (5.31)$$

where

$$E_{\pm}(\mathbf{r}, \omega) = \frac{E_x(\mathbf{r}, \omega) \mp iE_y(\mathbf{r}, \omega)}{\sqrt{2}}, \quad (5.32)$$

$$\hat{\mathbf{c}}_{\pm} = \frac{\hat{\mathbf{x}} \pm i\hat{\mathbf{y}}}{\sqrt{2}}, \quad (5.33)$$

the phase singularities of $E_+(\mathbf{r}, \omega)$ and $E_-(\mathbf{r}, \omega)$ may be found. In a color-coded plot of their phase, phase singularities are points where all colors meet. In Figs. 5.4 and 5.5, the phases are shown in the plane $z = 1$ m. The location of the C -points may be found approximately by again using Eq. (5.23) and solving for cases when $E_{\pm} = 0$. These are points (x, y) in the plane $z = z_0$ that simultaneously satisfy the two conditions

$$\frac{y}{z_0} = \frac{m\lambda}{3d}, \quad (5.34)$$

$$\frac{x}{z_0} = \frac{\beta_{mn}\lambda}{\pi\sqrt{3}d}, \quad (5.35)$$

where β_{mn} is the n^{th} solution to $|\sqrt{3}\sin\beta_{mn}| = |1 - (-1)^m \cos\beta_{mn}|$ and m and n are integers. Each m and n label a C -point in the region of interest.

The condition for L -lines and C -points are trivially met by the case $\mathbf{E} = 0$ (a V -point). In fact, co-location of phase singularities for both E_+ and E_- is a necessary and sufficient condition for the existence of a V -point. Likewise, a V -point can be thought of as the intersection of an L -line with a C -point. Inspection of Figs. 5.4 and 5.5 shows many locations beyond $(x, y) = (0, 0)$ that seem likely candidates for a V -point. However, it follows from symmetry considerations that such a point can only occur on the z -axis. Indeed it is found that the C -points are all slightly off to the side of the L -lines. The two types of singularities can only be shown to be co-located within the validity of the paraxial approximation — when $\sin\beta_{mn} = 0$ in Eq. (5.35). The pairs of C -points that are adjacent to the intersection of three L -lines are of opposite topological charge — their phases circulate in opposite directions. This implies that half of them are ‘star’-type C -points and the other half are either ‘lemon’- or ‘monstar’-type C -points [DENNIS, 2008]. The C -points that are not near an L -line intersection alternate between being ‘stars’ and ‘lemons’ along any of the three axes of symmetry. For example, between the two vertical L -lines located near $x = -0.7$ mm and $x = -0.4$ mm, the C -point near $y = -0.9$ mm is a ‘lemon’, the one above it is a ‘star’, and they alternate as the vertical position increases.

An alternative way of locating C -points is by plotting the phase of the quantity $\psi = \mathbf{E}(\mathbf{r}, \omega) \cdot \mathbf{E}(\mathbf{r}, \omega)$ [BERRY AND DENNIS, 2001]. This is done in Fig. 5.6. The advantage of this approach is that both left-handed and right-handed C -points are

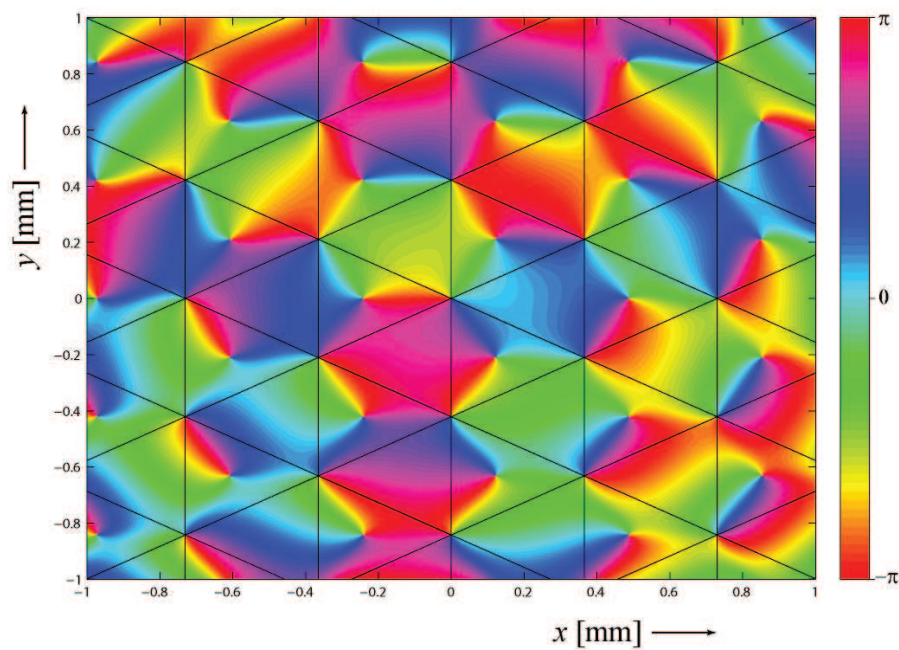


Figure 5.4: The phase of $E_+(\mathbf{r}, \omega)$ in the $z = 1$ m plane for the symmetric three-pinhole experiment. In this example $d = 1$ mm and $\lambda = 632.8$ nm. The phase singularities, points where all colors meet, correspond to C -points, i.e., points of left-handed circular polarization.

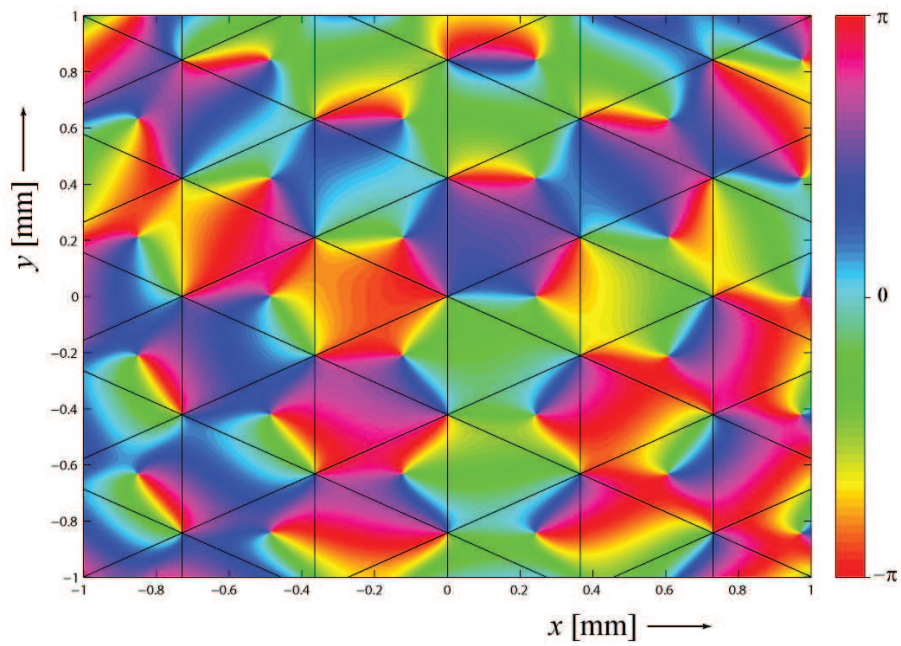


Figure 5.5: The phase of $E_-(\mathbf{r}, \omega)$ in the $z = 1$ m plane for the symmetric three-pinhole experiment. In this example $d = 1$ mm and $\lambda = 632.8$ nm. The phase singularities, points where all colors meet, correspond to C -points, i.e., points of right-handed circular polarization.

now simultaneously visible as phase singularities of ψ . These singularities have a charge that is twice the C -point charge, with the sign of the charge being positive (negative) for right-handed (left-handed) polarization.

The symmetry in the three-pinhole arrangement as presented above is not necessary to create such a rich topology of singular structures. As an example of a configuration where the pinhole locations are not symmetric, we consider the case where

$$\mathbf{r}_1 = d(0.8, 1, 0), \quad \mathbf{r}_2 = d(1, 0, 0), \quad \mathbf{r}_3 = d(0, 0, 0). \quad (5.36)$$

and

$$\hat{\mathbf{e}}_1 = (0, 1, 0), \quad \hat{\mathbf{e}}_2 = (0.8, -0.6, 0), \quad \hat{\mathbf{e}}_3 = \left(\frac{\sqrt{3}}{2}, \frac{-1}{2}, 0 \right). \quad (5.37)$$

Again, the field at each pinhole is taken to be of equal amplitude and co-phasal, and so Eq. (5.22) still applies. In Fig. 5.7, the spectral density of the field is shown in the plane $z = 1$ m. The V -point (a point of zero spectral density) has disappeared. Also, the pattern of L -lines is changed as compared to the symmetric case, with the lines no longer crossing each other. In Fig. 5.8, the phases of $E_+(\mathbf{r}, \omega)$ and $E_-(\mathbf{r}, \omega)$ are shown. Breaking the symmetry in pinhole locations changes the number of C -points and L -lines in a region, but it does not result in their disappearance. The occurrence of L -lines and C -points may therefore be said to be generic. Note that the two figures are no longer mirror images of one another - the location of a phase singularity of $E_+(\mathbf{r}, \omega)$ is no longer indicative of a location of a phase singularity of $E_-(\mathbf{r}, \omega)$. It is seen that linear polarization and both types of circular polarization can all occur in the vicinity of points of near-zero spectral density.

5.4 An N -pinhole interferometer

Young's experiment can be easily generalized from Eqs. (5.3) and (5.22) by changing the bound on the summation to N . The number of free parameters (e.g., the state of polarization of the electric field at each pinhole, and the location of the pinholes) make any absolute statement about the scalability of the previous analysis impossible. However, if the phase and amplitude of the field at each pinhole are the same, and the direction of linear polarization and the location of the pinholes are radially symmetric, a pattern does emerge. The V -line $x = 0, y = 0$ is present for all $N \geq 3$. In any transverse observation plane, an N -fold symmetry exists in the location of L -lines and C -points. This is illustrated in Fig. 5.9 where plots of S_0 and the phase of $E_-(\mathbf{r}, \omega)$ are shown for the cases $N = 4$ and $N = 7$. The phase of $E_+(\mathbf{r}, \omega)$ can be inferred from the phase of E_- through symmetry considerations.

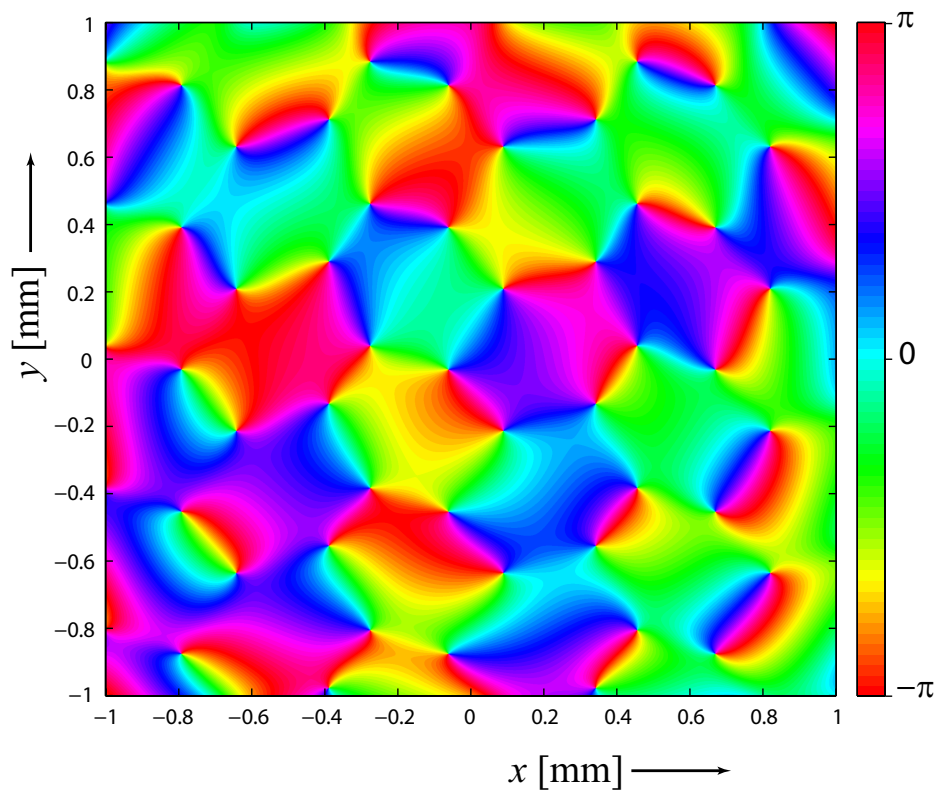


Figure 5.6: The phase of $\psi = \mathbf{E} \cdot \mathbf{E}$. All C -points coincide with phase singularities of the quantity ψ . In this example $d = 1$ mm and $\lambda = 632.8$ nm.

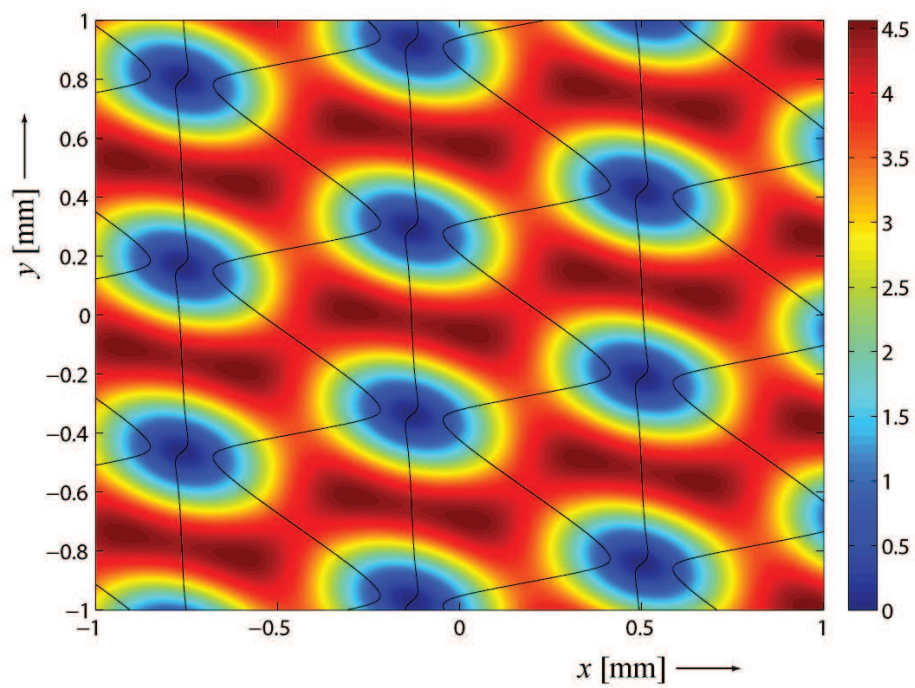


Figure 5.7: The spectral density in the $z = 1$ m plane for an asymmetric three-pinhole experiment. The solid black curves are lines of linear polarization. In this example $d = 1$ mm and $\lambda = 632.8$ nm.

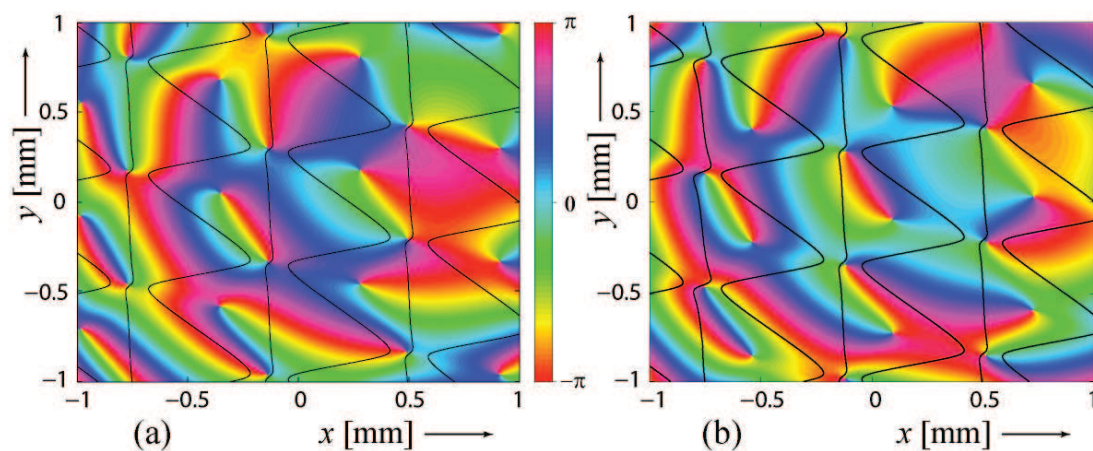


Figure 5.8: (The phase of $E_-(\mathbf{r}, \omega)$ [panel (a)], and the phase of $E_+(\mathbf{r}, \omega)$ [panel(b)] in the $z = 1$ m plane for an asymmetric three-pinhole configuration with $d = 1$ mm and $\lambda = 632.8$ nm.

5.5 Conclusion

We have studied the superposition of N linearly polarized fields in an N -pinhole interferometer. Despite the absence of interference fringes when fields with two orthogonal polarization states are used, the two-pinhole case still yields an interesting structure of a finite number of semi-hyperboloids on which the state of polarization is linear. The three-pinhole interferometer gives a much richer topological behaviour. L -lines and C -points were identified, and their occurrence was found to be generic. The generalization to an N -pinhole configuration was discussed for the case of a radially symmetric system.

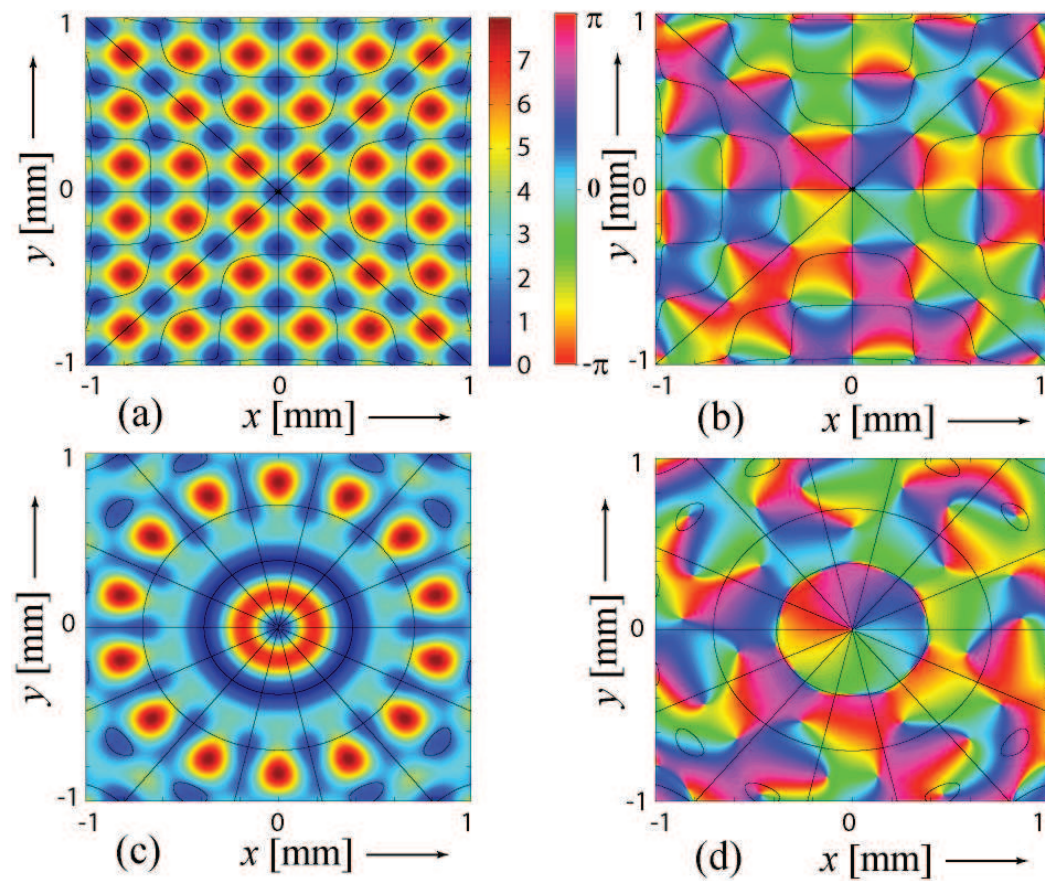


Figure 5.9: The spectral density (a) and the phase of $E_-(\mathbf{r}, \omega)$ (b) for the four-pinhole case, and for the seven-pinhole case (panels c,d), both in the $z = 1$ m plane with $d = 1$ mm and $\lambda = 632.8$ nm.

Bibliography

- G.S. AGARWAL, A. DOGARIU, T.D. VISSER, AND E. WOLF, “Generation of complete coherence in Young’s interference experiment with random mutually uncorrelated electromagnetic beams”, *Opt. Lett.* 30, 2, pp. 120–122 (2005).
- D. AMBROSINI, F. GORI, AND D. PAOLETTI, “Destructive interference from three partially coherent point sources”, *Opt. Commun.* 254, 1-3, pp. 30–39 (2005).
- C.A. BALANIS, *Advanced Engineering Electromagnetics*, Wiley New York (1989).
- L. BASANO AND P. OTTONELLO, “Complete destructive interference of partially coherent sources of acoustic waves”, *Phys. Rev. Lett.* 94, 17, 173901–173901 (2005).
- M.V. BERRY AND M.R. DENNIS, “Polarization singularities in isotropic random vector waves”, *Proc. R. Soc. Lond. A* 457, pp. 141–155 (2001).
- G.V. BOGATYRYOVA, C.V. FEL’DE, P.V. POLYANSKII, S.A. PONOMARENKO, M.S. SOSKIN, AND E. WOLF, “Partially coherent vortex beams with a separable phase”, *Opt. Lett.* 28, 11, pp. 878–880 (2003).
- G.V. BOGATYRYOVA, K.V. FELDE, P.V. POLYANSKII, AND M.S. SOSKIN, “Nongeneric polarization singularities in combined vortex beams”, *Optics and Spectroscopy* 97, 5, pp. 782–789 (2004).
- M. BORN AND E. WOLF, *Principles of Optics: Electromagnetic Theory of Propagation, Interference and Diffraction of Light*, Seventh (expanded) edition, Cambridge University Press, Cambridge (1999).
- C. BROSSEAU, *Fundamentals of Polarized Light*, Wiley New York (1998).
- W.H. CARTER AND E. WOLF, “Correlation theory of wavefields generated by fluctuating, three-dimensional, primary, scalar sources. II. Radiation from isotropic model sources”, *Opt. Acta* 28, 2, pp. 245–259 (1981).

- W.C. CHEW, *Waves and Fields in Inhomogeneous Media* (1995).
- E.T. COPSON, *An Introduction to the Theory of Functions of a Complex Variable*, Clarendon Press, London (1935).
- B.J. DAVIS AND P.S. CARNEY, “Robust determination of the anisotropic polarizability of nanoparticles using coherent confocal microscopy”, *J. Opt. Soc. Am. A* 25, 8, pp. 2102–2113 (2008).
- M.R. DENNIS, “Polarization singularities in paraxial vector fields: Morphology and statistics”, *Opt. Commun.* 213, pp. 201–221 (2002).
- M.R. DENNIS, “Polarization singularity anisotropy: determining monstardom”, *Opt. Lett.* 33, 22, pp. 2572–2574 (2008).
- D.W. DIEHL, R.W. SCHOONOVER, AND T.D. VISSER, “The structure of focused, radially polarized fields”, *Opt. Express* 14, 7, pp. 3030–3038 (2006).
- D.W. DIEHL AND T.D. VISSER, “Phase singularities of the longitudinal field components in high-aperture systems”, *J. Opt. Soc. Am. A* 21, pp. 2103–2108 (2004).
- T. VAN DIJK, H.F. SCHOUTEN, AND T.D. VISSER, “Coherence singularities in the far field generated by partially coherent sources”, *Phys. Rev. A* 79, 033805 (2009).
- T. VAN DIJK AND T.D. VISSER, “Evolution of singularities in a partially coherent vortex beam”, *J. Opt. Soc. Am. A* 26, pp. 741–744 (2009).
- A. EINSTEIN, “Méthode pour la détermination de valeurs statistiques d’observation concernant des grandeurs soumises a des fluctuations irrégulières”, *Arch. Sci. Phys. et Natur.* 37, pp. 254–256 (1914).
- D.G. FISCHER AND B. CAIRNS, “Inverse problems with quasihomogeneous random media utilizing scattered pulses”, *Journal of Modern Optics* 42, 3, pp. 655–666 (1995).
- D.G. FISCHER AND T.D. VISSER, “Spatial correlation properties of focused partially coherent light”, *J. Opt. Soc. Am. A* 21, 11, pp. 2097–2102 (2004).
- F. FLOSSMANN, U.T. SCHWARZ, M. MAIER, AND M.R. DENNIS, “Polarization singularities from unfolding an optical vortex through a birefringent crystal”, *Phys. Rev. Lett.* 95, 253901 (2005).

- F. FLOSSMANN, U.T. SCHWARZ, M. MAIER, AND M.R. DENNIS, “Stokes parameters in the unfolding of an optical vortex through a birefringent crystal”, *Optics Express* 14, 23, pp. 11402–11411 (2006).
- I. FREUND, “Polarization singularity indices in Gaussian laser beams”, *Opt. Commun.* 201, 4, pp. 251–270 (2002).
- I. FREUND, A.I. MOKHUN, M.S. SOSKIN, O.V. ANGELSKY, AND I.I. MOKHUN, “Stokes singularity relations”, *Opt. Lett.* 27, 7, pp. 545–547 (2002).
- C.H. GAN AND G. GBUR, “Phase and coherence singularities generated by the interference of partially coherent fields”, *Opt. Commun.* 280, 2, pp. 249–255 (2007).
- G. GBUR, “Nonradiating sources and other invisible objects”, In: E. Wolf, editor, *Progress in Optics*, volume 45, pp. 273–315, Elsevier Science (2003).
- G. GBUR AND G.A. SWARTZLANDER, “Complete transverse representation of a correlation singularity of a partially coherent field”, *J. Opt. Soc. Am. B* 25, 9, pp. 1422–1429 (2008).
- G. GBUR AND T.D. VISSER, “Coherence vortices in partially coherent beams”, *Opt. Commun.* 222, pp. 117–125 (2003).
- G. GBUR AND T.D. VISSER, “Phase singularities and coherence vortices in linear optical systems”, *Opt. Commun.* 259, pp. 428–435 (2005).
- G. GBUR, T.D. VISSER, AND E. WOLF, “Anomalous behavior of spectra near phase singularities of focused waves”, *Phys. Rev. Lett.* 88, 1, 013901 (2001).
- G. GBUR, T.D. VISSER, AND E. WOLF, “Complete destructive interference of partially coherent fields”, *Opt. Commun.* 239, 1-3, pp. 15–23 (2004a).
- G. GBUR, T.D. VISSER, AND E. WOLF, “‘Hidden’ singularities in partially coherent wavefields”, *J. Opt. A: Pure Appl. Opt.* 6, 5, pp. 239–242 (2004b).
- R. HANBURY BROWN AND R.Q. TWISS, “A new type of interferometer for use in radio-astronomy”, *Philos. Mag* 45, pp. 663–682 (1954).
- J.H. HANNAY, “The Majorana representation of polarization, and the Berry phase of light”, *J. Mod. Opt.* 45, 5, pp. 1001–1008 (1998).
- C. HUYGHENS, *Traité de la Lumière*, van der Aa, Leiden (1690).
- J.D. JACKSON, *Classical Electrodynamics*, second edition, John Wiley & Sons, New York (1975).

- G.P. KARMAN, M.W. BEIJERSBERGEN, A. VAN DUIJL, AND J.P. WOERDMAN, “Creation and annihilation of phase singularities in a focal field”, *Opt. Lett.* 22, pp. 1503–1505 (1997).
- G.P. KARMAN, A. VAN DUIJL, AND J.P. WOERDMAN, “Unfolding of an unstable singularity point into a ring”, *Opt. Lett.* 23, 6, pp. 403–405 (1998).
- A. KHINTCHINE, “Korrelationstheorie der stationären stochastischen Prozesse”, *Math. Ann.* 109, 1, pp. 604–615 (1934).
- N. KUZMIN, G.W. 'T HOOFT, E.R. ELIEL, G. GBUR, H.F. SCHOUTEN, AND T.D. VISSER, “Enhancement of spatial coherence by surface plasmons”, *Opt. Lett.* 32, 5, pp. 445–447 (2007).
- H.A. LORENTZ, “Über die Beziehung zwischen der Fortpflanzung des Lichtes und der Körperdichte”, *Wiedemann Ann* 9, pp. 641–664 (1880).
- L. LORENZ, “Über die Refraktionsconstante”, *Ann. Phys* 11, pp. 70–103 (1881).
- R. LOUDON, *The Quantum Theory of Light*, Third edition, Oxford University Press (2003).
- I.D. MALEEV AND G.A. SWARTZLANDER, JR, “Propagation of spatial correlation vortices”, *J. Opt. Soc. Am. B* 25, 6, pp. 915–922 (2008).
- L. MANDEL AND E. WOLF, *Optical Coherence and Quantum Optics*, Cambridge University Press (1995).
- J.C. MAXWELL, *A Treatise on Electricity and Magnetism*, Clarendon (1892).
- A.A. MICHELSON AND F.G. PEASE, “Measurement of the diameter of Alpha-Orionis by the interferometer”, *Proc. Natl. Acad. Sci.* 7, 5, pp. 143–146 (1921).
- A.I. MOKHUN, M.S. SOSKIN, AND I. FREUND, “Elliptic critical points: C-points, a-lines, and the sign rule”, *Opt. Lett.* 27, 12, pp. 995–997 (2002).
- M. MUJAT, A. DOGARIU, AND E. WOLF, “A law of interference of electromagnetic beams of any state of coherence and polarization and the Fresnel-Arago interference laws”, *J. Opt. Soc. Am. A* 21, 12, pp. 2414–2417 (2004).
- L. NOVOTNY, M.R. BEVERSLUIS, K.S. YOUNGWORTH, AND T.G. BROWN, “Longitudinal field modes probed by single molecules”, *Phys. Rev. Lett.* 86, 23, 5251–5254 (2001).

- J.F. NYE, *Natural Focusing and Fine Structure of Light*, IOP Publishing, Bristol (1999).
- J.F. NYE AND M.V. BERRY, “Dislocations in wave trains”, *Proc. R. Soc. Lond. A* 336, pp. 165–190 (1974).
- D.M. PALACIOS, I.D. MALEEV, A.S. MARATHAY, AND G.A. SWARTZLANDER JR, “Spatial correlation singularity of a vortex field”, *Phys Rev Lett* 92, pp. 143905 (2004).
- B. RICHARDS AND E. WOLF, “Electromagnetic diffraction in optical systems. II. Structure of the image field in an aplanatic system”, *Proc. R. Soc. Lond. A* 253, 1274, pp. 358–379 (1959).
- H. ROYCHOWDHURY AND E. WOLF, “Young’s interference experiment with light of any state of coherence and of polarization”, *Opt. Commun.* 252, 4-6, pp. 268–274 (2005).
- G. RUBEN AND D.M. PAGANIN, “Phase vortices from a Young’s three-pinhole interferometer”, *Phys. Rev. E* 75, 6, 66613 (2007).
- R.W. SCHOONOVER AND T.D. VISSER, “Polarization singularities of focused, radially polarized fields”, *Opt. Express* 14, 12, pp. 5733–5745 (2006).
- H.F. SCHOUTEN, G. GBUR, T.D. VISSER, AND E. WOLF, “Phase singularities of the coherence functions in Young’s interference pattern”, *Opt. Lett.* 28, pp. 968–970 (2003a).
- H.F. SCHOUTEN, N. KUZMIN, G. DUBOIS, T.D. VISSER, G. GBUR, P.F.A. ALKEMADE, H. BLOK, G.W. HOOFT, D. LENSTRA, AND E.R. ELIEL, “Plasmon-assisted two-slit transmission: Young’s experiment revisited”, *Phys. Rev. Lett.* 94, 053901 (2004a).
- H.F. SCHOUTEN, T.D. VISSER, G. GBUR, D. LENSTRA, AND H. BLOK, “Creation and annihilation of phase singularities near a sub-wavelength slit”, *Opt. Express* 11, 4, pp. 371–380 (2003b).
- H.F. SCHOUTEN, T.D. VISSER, G. GBUR, D. LENSTRA, AND H. BLOK, “The diffraction of light by narrow slits in plates of different materials”, *J. Opt. A: Pure Appl. Opt.* 6, pp. 277–280 (2004b).
- H.F. SCHOUTEN, T.D. VISSER, D. LENSTRA, AND H. BLOK, “Light transmission through a subwavelength slit: Waveguiding and optical vortices”, *Phys. Rev. E* 67, 3, 36608 (2003c).

- H.F. SCHOUTEN, T.D. VISSER, AND E. WOLF, “New effects in Young’s interference experiment with partially coherent light”, *Opt. Lett.* 28, 14, pp. 1182–1184 (2003d).
- T. SETALA, J. TERVO, AND A.T. FRIBERG, “Contrasts of Stokes parameters in Young’s interference experiment and electromagnetic degree of coherence”, *Opt. Lett.* 31, 18, pp. 2669–2671 (2006).
- M.S. SOSKIN, V. DENISENKO, AND I. FREUND, “Optical polarization singularities and elliptic stationary points”, *Opt. Lett.* 28, 16, pp. 1475–1477 (2003).
- M.S. SOSKIN, P.V. POLYANSKII, AND O.O. ARKHELYUK, “Computer-synthesized hologram-based rainbow optical vortices”, *New Jnl. of Physics* 6, 1, pp. 196 (2004).
- M.S. SOSKIN AND M.V. VASNETSOV, “Singular optics”, In: E. Wolf, editor, *Progress in Optics*, volume 42, pp. 219–276, Elsevier Science (2001).
- G.G. STOKES, “On the composition and resolution of streams of polarized light from different sources”, *Trans. Cambr. Phil. Soc.* page 399 (1852).
- G.A. SWARTZLANDER AND J. SCHMIT, “Temporal correlation vortices and topological dispersion”, *Phys. Rev. Lett.* 93, 93901–93901 (2004).
- C. TAI, *Dyadic Green Functions in Electromagnetic Theory*, IEEE Press, Piscataway, NJ (1994).
- B.J. THOMPSON AND E. WOLF, “Two-beam interference with partially coherent light”, *J. Opt. Soc. Am.* 47, 10, pp. 895 (1957).
- T.D. VISSER AND J.T. FOLEY, “On the wavefront spacing of focused, radially polarized beams”, *J. Opt. Soc. Am. A* 22, 11, pp. 2527–2531 (2005).
- T.D. VISSER AND R.W. SCHOONOVER, “A cascade of singular field patterns in Young’s interference experiment”, *Opt. Commun.* 281, 1, pp. 1–6 (2008).
- W. WANG, Z. DUAN, S.G. HANSON, Y. MIYAMOTO, AND M. TAKEDA, “Experimental study of coherence vortices: Local properties of phase singularities in a spatial coherence function”, *Phys. Rev. Lett.* 96, 073902 (2006).
- W. WANG, A.T. FRIBERG, AND E. WOLF, “Focusing of partially coherent light in systems of large Fresnel numbers”, *J. Opt. Soc. Am. A* 14, 2, pp. 491–496 (1997).

- N. WIENER, “Generalized harmonic analysis”, *Acta Math.* 55, 1, pp. 117–258 (1930).
- E. WOLF, “A macroscopic theory of interference and diffraction of light from finite sources. ii. fields with a spectral range of arbitrary width”, *Proc. R. Soc. Lon. A* 230, 1181, pp. 246–265 (1955).
- E. WOLF, “New spectral representation of random sources and of the partially coherent field that they generate”, *Opt. Commun.* 38, pp. 3–6 (1981).
- E. WOLF, “New theory of partial coherence in the space-frequency domain. part I: spectra and cross spectra of steady-state sources”, *J. Opt. Soc. Am.* 72, pp. 343–351 (1982).
- E. WOLF, “Invariance of the spectrum of light on propagation”, *Phys. Rev. Lett.* 56, 13, 1370–1372 (1986).
- E. WOLF, “Unified theory of coherence and polarization of random electromagnetic beams”, *Phys. Lett. A* 312, pp. 263–267 (2003).
- E. WOLF, *Introduction to the Theory of Coherence and Polarization*, Cambridge University Press (2007).
- E. WOLF AND D.F.V. JAMES, “Correlation-induced spectral changes”, *Rep. on Prog. in Phys.* 59, pp. 771–818 (1996).
- T. YOUNG, “The Bakerian lecture: Experiments and calculations relative to physical optics”, *Phil. Trans. R. Soc. Lond* 94 (1804).
- T. YOUNG, *A Course of Lectures on Natural Philosophy and the Mechanical Arts*, 2 Vols., Johnson, London (1807).
- K.S. YOUNGWORTH AND T.G. BROWN, “Focusing of high numerical aperture cylindrical-vector beams”, *Opt. Express* 7, 2, pp. 77–87 (2000).
- F. ZERNIKE, “The concept of degree of coherence and its application to optical problems”, *Physica* 5, pp. 785–795 (1938).

Appendix A

Mathematical Derivations

A.1 The sign rule

The general sign rule, as derived in [FREUND *et al.*, 2002], is

$$2\sigma_k \sum_{(k)} q_{ij} = \sum^{(k)} \sigma_i q_{jk}, \quad (\text{A.1})$$

where $\sum_{(k)}$ is used to denote the sum of singularities enclosed by the line Z_k (level curves $S_k = 0$) and $\sum^{(k)}$ is used to denote the sum of singularities on the line Z_k . Also, $\sigma_i = \text{sign}(S_i)$ and q_{ij} is the topological charge of a singularity of the Stokes scalar $S_{ij} = S_i + iS_j$. In looking for the relationship between L -lines and C -points, only $k = 3$ (L -lines) are of importance. In the configuration specific to this class of problems, L -lines enclose only right-handed circular points (singularities of e_-); therefore, $\sigma_3 = 1$. Equation (A.1) then simplifies to

$$2 \sum_{\in L} q_{12} = \sum_L \sigma_1 q_{23}. \quad (\text{A.2})$$

By rewriting the Stokes parameters from Eqs. (3.19)-(5.10)

$$S_1 = |e_z|^2 - |e_\rho|^2, \quad (\text{A.3})$$

$$S_2 = 2\text{Re}\{e_z^* e_\rho\}, \quad (\text{A.4})$$

$$S_3 = 2\text{Im}\{e_z^* e_\rho\}, \quad (\text{A.5})$$

it is obvious that $\sigma_1 = 1$ for singularities of e_ρ and $\sigma_1 = -1$ for singularities of e_z . Also, it is readily apparent that $S_{23} = 2e_z^* e_\rho$. Thus, $q_{23} = q_\rho$ when the singularity is in e_ρ and $q_{23} = -q_z$ when the singularity is in e_z . Finally, it is necessary to find

the relationship between q_{12} and singularities in e_- . By writing

$$e_\rho = \frac{e_- - e_+}{i\sqrt{2}}, \quad (\text{A.6})$$

$$e_z = \frac{e_- + e_+}{\sqrt{2}}, \quad (\text{A.7})$$

and inserting these relations into Eqs. (A.3-A.5) it is seen that

$$S_1 = 2\text{Re}\{e_+^*e_-\}, \quad (\text{A.8})$$

$$S_2 = 2\text{Im}\{e_+^*e_-\}, \quad (\text{A.9})$$

$$S_3 = |e_-|^2 - |e_+|^2, \quad (\text{A.10})$$

and that $S_{12} = 2e_+^*e_-$. Therefore, $q_{12} = q_-$ when the singularity is in e_- and the sum rule is

$$2 \sum_{\text{enclosed}} q_- = \sum_{\text{on}} q_\rho + \sum_{\text{on}} q_z. \quad (\text{A.11})$$

A.2 Degeneracy of linear polarization states for the two-pinhole interferometer

Any choice for the direction of linear polarization of the electric field at the two pinholes may, without loss of generality, be described as

$$\hat{\mathbf{e}}_1 = \hat{\mathbf{x}}, \quad \hat{\mathbf{e}}_2 = \cos \alpha \hat{\mathbf{x}} + \sin \alpha \hat{\mathbf{y}}. \quad (\text{A.12})$$

On substitution in Eqs. (3.11) and (5.10), and imposing the condition for linear polarization (*i.e.* $S_3 = 0$), we obtain the expression

$$\sin \alpha \sin[k(R_2 - R_1)] = 0. \quad (\text{A.13})$$

This condition can be satisfied when $\alpha = 0$, which is the trivial case in which the field at both pinholes is x -polarized. The second solution, $k(R_2 - R_1) = m\pi$, with n an integer, is identical to Eq. (5.11), and results in surfaces of linear polarization. Note that relaxing the condition that the field in each pinhole is co-phasal with each other changes the condition for linear polarization to $kR_1 - kR_2 = n\pi + \beta$, where β is the relative phase. This equation still yields a collection of hyperboloids, although the plane at $x = 0$ is now no longer an L -surface.

For circular polarization to occur, the field must satisfy $E_x(\mathbf{r}, \omega) = \pm iE_y(\mathbf{r}, \omega)$. Again using Eq. (A.12), a simple calculation yields the conditions $R_1 = R_2$ and $\alpha = \pi$. These two conditions actually result in $\mathbf{E} = 0$ on the plane $x = 0$. A

surface of circular polarization can be created by relaxing the condition that the field in each pinhole is of equal amplitude. Instead, if the field amplitudes in the two pinholes have a ratio $|E_x|/|E_y| = \gamma$ such that γ simultaneously solves $R_1 = \gamma R_2$ and $(\gamma - 1)kR_2 = (2n + 1)\pi/2$ for some integer n at a point \mathbf{r} , then the conditions for circular polarization can be met on, at most, a single hyperboloid.

Summary

In this Thesis, a broad class of optical phenomena have been investigated, including the power radiated by two correlated sources, the fine structure of an optical field in the focal region, the relationship between singular structures for various types of optical fields, and the state of polarization in a three-pinhole experiment. The topics are all related through the unified theory of coherence and polarization, and the investigations are aided by the using the tools of singular optics. Singular optics allows for an investigation into the smallest structures in an optical field - phenomena occurring on a scale well below the diffraction limit, yet made 'observable' through knowledge of the field patterns near a singular point.

The total power radiated by two correlated sources is investigated in Chapter 2. It is shown that the total power for two primary or secondary sources is a function of both the distance between the two sources and the spectral degree of coherence between the two sources. When two primary sources are highly correlated and close (say, on the order of a wavelength), the total power radiated by the system approaches double the power radiated when the two sources are either separated by a large distance or if the two sources are uncorrelated. One notes that in the case of a planar, secondary source, the total power obeys a similar relationship, although the functional dependence is slightly different.

In Chapter 3, the fine structure of radially polarized optical fields in the focal region are investigated. First, the energy density is shown to be a strong function of the semi-aperture angle of the lens (the numerical aperture). Using the tools of singular optics, the phase structure of each field component is explored, and the creation and annihilation of phase singularities are observed. The state of polarization is investigated in the focal region. It is shown that the field in the focal region has a number of polarization singularities, including points of circular polarization and lines of linear polarization, and creation and annihilation of circular polarization states are observed. It is also shown that a V -point, a point where there is no electric field, may exist in the focal region.

The relationship between the various types of singular structures is found in Chapter 4. In this Chapter, a two-pinhole interferometer is illuminated by three different types of fields - a scalar, stochastic field; a scalar, deterministic field; and

a polarized, deterministic field - and the resulting field patterns are investigated. It is shown that, as the magnitude of the degree of coherence between the field in the two pinholes is increased from zero to one, a pair of coherence vortices move closer together. In the deterministic limit, the pairs of coherence vortices merge into phase vortices. The scalar, deterministic model is often valid when the field is linearly polarized in an isotropic medium. By changing the state of polarization in the pinholes, the field at the location of the phase singularity unfolds into three vector singularities, two oppositely-handed points of circular polarization and a point of linear polarization.

The state of polarization emanating from an N -pinhole interferometer is examined in Chapter 5. It is shown that circular polarization states do not exist for a two-pinhole interferometer, except in a contrived case. A collection of surfaces (hyperboloids) on which the field is linearly polarized exist generically in the two-pinhole case. For a three-pinhole interferometer, linear and circular polarization states exist generically. For a highly symmetric configuration - when the pinholes are placed at the vertex of an equilateral triangle and the field at each pinhole is polarized in a direction parallel to the line between the origin and the vertex - the field on a plane parallel to the interferometer plane contains a regular pattern of lines of linear polarization and points of circular polarization. The center of the observation plane contains a single V -point. For more than three pinholes, it is shown that a highly symmetric configuration still yields a regular pattern of circular and linear polarization states, with a single V -point at the origin.

These previous investigations in singular optics are unified through the theory of coherence and polarization. Using Maxwell's equations and coherence theory, the fine structure of optical fields has been examined for a number of optical systems, particularly interferometers and lenses, and a number of relationships have been established between the singular structures and the fields that generate them.

List of Publications

- **R.W. Schoonover**, J.M. Rutherford, O. Keller, P.S. Carney, “Nonlocal constitutive relations and the quasi-homogeneous approximation,” *Phys. Lett. A.* **342**, 363-367 (2005).
- D.W. Diehl, **R.W. Schoonover**, and T.D. Visser, “The structure of focused, radially polarized fields,” *Opt. Express* **14**, 3030–3038 (2006)
- **R.W. Schoonover** and T.D. Visser, “Polarization singularities of focused, radially polarized fields,” *Opt. Express* **14**, 5733–5745 (2006).
- **R.W. Schoonover**, T.D. Visser, “The power radiated by two correlated sources,” *Opt. Commun.* **271**, Issue 2, 323–326 (2007).
- T.D. Visser, **R.W. Schoonover**, “A cascade of singular field patterns in Young’s interference experiment,” *Opt. Commun.* **281**, Issue 1, 1–6 (2008).
- **R.W. Schoonover**, B.J. Davis, R.A. Bartels, P.S. Carney, “Optical interferometry with pulsed fields,” *Journ. Mod. Opt.*, **55**, 1541-1556 (2008).
- **R.W. Schoonover**, A.M. Zysk, P.S. Carney, J.C. Schotland, E. Wolf, “Geometrical limits of stochastic electromagnetic fields,” *Phys. Rev. A* **77**, 043831 (2008).
- **R.W. Schoonover**, B.J. Davis, P.S. Carney, “The generalized Wolf shift for cyclostationary fields,” *Opt. Express* **17**, 4705–4711 (2009).
- B.J. Davis and **R.W. Schoonover**, “Computationally efficient methods for calculating coherent-mode representations,” *Opt. Lett.* **34**, 923–925 (2009).
- **R.W. Schoonover**, T.D. Visser, “Creating polarization singularities with an N -pinhole interferometer,” *Phys. Rev. A* **79**, 043809 (2009).
- **R.W. Schoonover**, B.J. Davis, R.A. Bartels, P.S. Carney, “Propagation of spatial coherence in fast pulses,” *submitted to J. Opt. Soc. Am. A.*

- P.S. Carney, N.D. Hardy, **R.W. Schoonover**, “Discrimination of single and multiple scattering by contrast modulation,” *in preparation*

Biography

Robert W. Schoonover was born in Macomb, IL in 1981, and lived there through much of his childhood. He attended St. Paul Elementary School and Macomb Jr.-Sr. High School. In 2000, he began interning for Motorola and enrolled at the University of Illinois, Urbana-Champaign (UIUC) to pursue a bachelor's degree in Electrical Engineering. Upon graduation in 2004, Robert enrolled in graduate school under the guidance of Prof. P. Scott Carney. In 2005, Robert won a Fulbright Scholarship to study at the Vrije Universiteit in The Netherlands under Prof. Taco Visser. Robert returned to UIUC in the summer of 2006 and completed his Master's degree in December. Robert will receive Ph.Ds from UIUC and the Delft University of Technology in 2009.

Acknowledgments

I am grateful to a number of people who have influenced me and this thesis.

My wife-to-be, Dr. Katrina Thomas, has shown great love and support for the past four years, and almost never complained when I left the country for long periods of time.

My family, especially my parents, for encouraging my curiosity from a young age. They've always been there when I've needed them.

The U.S. Fulbright Program allowed my work with Prof. Visser to begin, and for that I will always be thankful. The Netherlands Fulbright Program, especially Drs. Linda Pietersen, made my transition to the Netherlands painless.

Deborah Tedrick and Anja Visser have both been wonderful in how accepting they are of my presence at their houses at all hours, or when I am the reason their husbands are otherwise detained.

I owe much to Prof. Scott Carney. He introduced me to Prof. Visser and encouraged me to apply for a Fulbright Fellowship in the first place. Where other advisors might want their students to work only on projects for them, Scott let me work on other projects, as well, at the University of Illinois. I could not have asked for better from him.

Finally, Prof. Taco Visser, who has been an advisor, friend, and dinner companion. I will always have fond memories of eating dinner with him and talking about politics, life, and occasionally, science. My graduate studies have been all the richer from our collaboration.